Deperturbation analysis of the $A^1\Pi(v=2)$ level in the $^{12}C^{18}O$ isotopologue

 $\mbox{M.I. Malicka}$, S. Ryzner , A.N. Heays , N. de Oliveira , R.W. Field , W. Ubachs , R. Hakalla

PII: \$0022-4073(21)00330-7

DOI: https://doi.org/10.1016/j.jqsrt.2021.107837

Reference: JQSRT 107837

To appear in: Journal of Quantitative Spectroscopy & Radiative Transfer

Received date: 11 June 2021 Accepted date: 12 July 2021

Please cite this article as: M.I. Malicka, S. Ryzner, A.N. Heays, N. de Oliveira, R.W. Field, W. Ubachs, R. Hakalla, Deperturbation analysis of the $A^1\Pi(v=2)$ level in the $^{12}C^{18}O$ isotopologue, *Journal of Quantitative Spectroscopy & Radiative Transfer* (2021), doi: https://doi.org/10.1016/j.jqsrt.2021.107837

This is a PDF file of an article that has undergone enhancements after acceptance, such as the addition of a cover page and metadata, and formatting for readability, but it is not yet the definitive version of record. This version will undergo additional copyediting, typesetting and review before it is published in its final form, but we are providing this version to give early visibility of the article. Please note that, during the production process, errors may be discovered which could affect the content, and all legal disclaimers that apply to the journal pertain.

© 2021 Published by Elsevier Ltd.



Highlights

- VUV-FT (SOLEIL synchrotron) and VIS-FT (IFS-125HR, Bruker) techniques were applied.
- Spectra of the $B^1\Sigma^+$ - $A^1\Pi$, $C^1\Sigma^+$ - $A^1\Pi$ and $A^1\Pi$ - $X^1\Sigma^+$ transitions in ${}^{12}C^{18}O$ were recorded.
- The deperturbation analysis of the $A^1\Pi(v=2)$ level in $^{12}C^{18}O$ was performed.
- A significant, indirect influence of $a^3\Pi$ on the $A^1\Pi$ state was detected.
- Spin-orbit and rotation-electronic interactions within $A^1\Pi(v=2)$ were analysed.
- Terms of the A¹ Π , e³ Σ ⁻, I¹ Σ ⁻, a'³ Σ ⁺ and d³ Δ levels in ¹²C¹⁸O were determined.



Deperturbation analysis of the $A^1\Pi(v=2)$ level in the $^{12}C^{18}O$ isotopologue

M. I. Malicka¹, S. Ryzner², A. N. Heays³, N. de Oliveira⁴, R. W. Field⁵, W. Ubachs⁶ and R. Hakalla^{2,*}

ABSTRACT

The rotational structure of the $A^{1}\Pi(v=2)$ level of $^{12}C^{18}O$ is re-examined using high-accuracy experimental data comprised of 541 molecular lines obtained by two complementary Fouriertransform techniques. The far ultraviolet absorption spectrum of the $A^1\Pi - X^1\Sigma^+(2, 0)$ band, in the range 66,500 - 67,650 cm⁻¹, was recorded by the vacuum-ultraviolet FT spectrometer at the DESIRS beamline of the SOLEIL synchrotron. Visible emission spectra of the $B^1\Sigma^+ - A^1\Pi(0, 2)$ and $C^1\Sigma^+ A^{1}\Pi(0, 2)$ bands in the range 19,200 - 20,000 and 24,300 - 24,800 cm⁻¹ were obtained with a Bruker IFS-125HR spectrometer at the University of Rzeszów. The absolute accuracy of line frequencies are 0.01 and 0.005 - 0.01 cm⁻¹, respectively. Results from the $B^1\Sigma^+ - X^1\Sigma^+(0, 0)$ and $C^1\Sigma^+ - X^1\Sigma^+(0, 0)$ absorption bands of ¹²C¹⁸O were added to the experimental data set. A deperturbation analysis of $A^{1}\Pi(v=2)$ is performed with an effective Hamiltonian and a term-value fitting approach. Accurate molecular constants for $A^1\Pi(v=2)$ and the $e^3\Sigma^-(v=4)$, $d^3\Delta(v=7)$, $a'^3\Sigma^+(v=12)$ and $I^1\Sigma^-(v=3)$ perturbing levels were determined. Perturbation parameters of the spin-orbit $A^1\Pi(v=2) \sim [e^3\Sigma^-(v=4)]$, $d^3\Delta(v=7)$, $a'^3\Sigma^+(v=12)$] and rotation-electronic (*L*-uncoupling) $A^1\Pi(v=2) \sim [I^1\Sigma^-(v=3,4), D^1\Delta(v=1)]$ 3)] interactions, were obtained. A significant, indirect influence of the $a^3\Pi$ state on the $A^1\Pi$ state was detected in 12C18O and has therefore been included in the final fit by taking into account the simultaneous $a^{3}\Pi(v = 13) \sim [e^{3}\Sigma^{-}(v = 4), d^{3}\Delta(v = 7), a^{3}\Sigma^{+}(v = 12)] \sim A^{1}\Pi(v = 2)$ spin-orbit/spinelectronic/L-uncoupling and spin-orbit interactions as well as the $a^3\Pi(v=13) \sim [D^1\Delta(v=3), I^1\Sigma^-(v=1)]$ 3)] $\sim A^{1}\Pi(v=2)$ spin-orbit and L-uncoupling interactions. This work results in determination of 110 rotational term-values for the $A^{1}\Pi(v=2)$ state and its perturbers.

¹ The Faculty of Mathematics and Applied Physics, Rzeszów University of Technology, Powstańców Warszawy 8 Street, 35-959 Rzeszów, Poland.

² Materials Spectroscopy Laboratory, Institute of Physics, University of Rzeszów, Pigonia 1 Street, 35-310 Rzeszów, Poland.

³ J. Heyrovský Institute of Physical Chemistry, Dolejškova 2155/3, 182 23 Prague 8, Czech Republic.

⁴ Synchrotron SOLEIL, Orme de Merisiers, St. Aubin, BP 48, F-91192 Gif sur Yvette Cedex, France.

⁵ Department of Chemistry, Massachusetts Institute of Technology, Cambridge, MA02139 USA.

⁶ Department of Physics and Astronomy, and LaserLaB, Vrije Universiteit, De Boelelaan 1081, 1081 HV Amsterdam, Netherlands.

KEYWORDS:

VUV and VIS high-resolution Fourier-transform techniques;

CO;

Carbon monoxide;

¹²C¹⁸O isotopologue;

Deperturbation analysis;

Spin-orbit, spin-electronic and rotation-electronic (L-uncoupling) perturbations;

Significant indirect $a^3\Pi \sim A^1\Pi$ interaction.

* Corresponding author: R. Hakalla

E-mail address: hakalla@ur.edu.pl

1. Introduction

The CO $A^1\Pi$ state is a prototypical example of a perturbed diatomic-molecular state and is subject to complex intra-molecular interactions with the $a'^3\Sigma^+$, $e^3\Sigma^-$, $d^3\Delta$, and $a^3\Pi$ triplet states, and $I^1\Sigma^-$ and $D^1\Delta$ singlet states [1,2]. The importance of the CO $A^1\Pi - X^1\Sigma^+$ system as a sensitive probe of a molecular gas in the interstellar medium, including minor CO isotopologues, [3–5] is another reason for its continued study.

The first deperturbation analysis of $A^1\Pi$ vibrational states and their interactions with neighbouring levels was carried out for $^{12}C^{16}O$ by Field et al. [6,7] using grating-spectrometer data obtained with an accuracy of 0.1 cm^{-1} . Later, Le Floch et al. [8] observed $A^1\Pi - X^1\Sigma^+$ absorption and emission lines with an accuracy of 0.02 cm^{-1} and included observations of the $D^1\Delta$ state perturbing $A^1\Pi$ and higher rotational levels for $A^1\Pi(v=0-9)$ [8–10]. More recently, accurate deperturbation analyses were performed for the $A^1\Pi(v=0-1)$ [11] and $A^1\Pi(v=2-4)$ [12] states, employing the capabilities of two-photon Doppler-free laser spectroscopy and Fourier-transform (FT) vacuum-ultraviolet (VUV) synchrotron spectroscopy, having accuracies of 0.002 cm^{-1} and 0.01 cm^{-1} , respectively. These techniques were also combined with FT emission spectroscopy in the visible (VIS) region with an accuracy of 0.005 cm^{-1} and extended to the study of other carbon monoxide isotopologues. Deperturbation analyses were performed by Niu et al. [12] for $^{13}C^{16}O$ $A^1\Pi(v=0)$, and Hakalla et al. for $^{12}C^{17}O$ $A^1\Pi(v=1-5)$ [13], $^{13}C^{17}O$ $A^1\Pi(v=0-3)$ [14], and $^{13}C^{18}O$ $A^1\Pi(v=0)$ [15]. In the latter case of $^{13}C^{18}O$ already an indication for an indirect interaction between the CO $a^3\Pi$ and $A^1\Pi$ electronic states was observed and analysed.

As for the $^{12}C^{18}O$ isotolpologue deperturbation analyses of the $A^1\Pi(v=1 \text{ and } 2)$ levels were performed by Haridass et al. [16] based on emission spectra accurate to 0.1 cm⁻¹. Beaty et al. [17] probed the $A^1\Pi(v=0-9)$ levels observed in a supersonic jet expansion with an accuracy of 0.2 cm⁻¹. Trivikram et al. [18] analysed the $A^1\Pi(v=0)$ level from observations of $A^1\Pi - X^1\Sigma^+$, $B^1\Sigma^+ - X^1\Sigma^+$ and $B^1\Sigma^+ - A^1\Pi$ systems obtained by two-photon Doppler-free laser spectroscopy, VUV-FT synchrotron spectroscopy and VIS-FT emission spectroscopy with accuracies of 0.001 cm⁻¹, 0.01 and 0.005 cm⁻¹. Most recently, Malicka et al. [19] studied the $A^1\Pi(v=1)$ level in $B^1\Sigma^+ - A^1\Pi$ and $C^1\Sigma^+ - A^1\Pi$ emission spectra and measured frequencies accurate to 0.005 cm⁻¹, along with $A^1\Pi - X^1\Sigma^+$, $B^1\Sigma^+ - X^1\Sigma^+$ and $C^1\Sigma^+ - X^1\Sigma^+$ VUV absorption spectra at an accuracy of 0.01 cm⁻¹.

Our goal is to improve upon this analysis by using modern VUV-FT and VIS-FT techniques and perform a more accurate analysis than previously, deriving improved molecular constants and rotational term values of the $A^1\Pi(\nu=2)$ vibrational level and its perturbers as well as their mutual interaction energies. The extremely-high precision of the measured frequencies and the characterization of all direct interactions that affect the $A^1\Pi(\nu=2)$ level, made it possible for the first time to identify and fully characterization an indirect $a^3\Pi \sim A^1\Pi$ interaction in $^{12}C^{18}O$. Additionally, the new data extends to significantly higher rotational excitation than previously and are

photoelectrically detected so that line intensities are quantitatively measured. This work is a continuation of the research on the $A^1\Pi$ state of carbon monoxide conducted by our team in recent years [12–15,18,19].

2. Experimental details

2.1. High-resolution VUV-FT absorption spectroscopy (SOLEIL synchrotron)

Vacuum-ultraviolet (VUV) photo-absorption spectra of the $A^1\Pi - X^1\Sigma^+(2, 0)$ band were recorded with the all-reflection Fourier-transform spectrometer on the DESIRS beamline of the SOLEIL synchrotron [20,21]. The methodology of these measurements, including the option for maintaining a high temperature, and their analysis is the same as that used in our previous study of the $^{13}C^{18}O$ $A^1\Pi - X^1\Sigma^+(0, 0)$ band [15]. Briefly, for this study, an isotopically-enriched sample of $^{12}C^{18}O$ was flowing into 20 cm-long T-shaped windowless cell placed in vacuum into the synchrotron beam path. The cell can be heated up thanks to a heating element closely wrapped around it. Post-analysis revealed 1% contamination by $^{12}C^{16}O$ in the sample that was observable in some measurements, and less than 0.5% for any other isotopologue.

Measurements were made at a temperature of 850 K and with approximate CO pressures of 0.03 and 0.4 hPa, corresponding to measured column densities of 4×10¹⁴ and 8×10¹⁵ cm⁻². These spectra are shown in Fig. 1 and were simultaneously fit to a model of all $A^1\Pi - X^1\Sigma^+$ and forbidden transitions. The frequencies and strengths of all lines were optimised taking into account overlapping absorption by ¹²C¹⁶O and instrumental broadening. Additionally, the relative frequencies of P- and Rbranch lines that terminate on a common upper level were kept fixed to their expected combination difference based on their extremely well-known ground-state energy levels. These are computed by Coxon et al. [22] that reproduce a large dataset of pure-rotational and ro-vibrational transitions frequencies for multiple isotopologues and with typical accuracies of 0.0001 cm⁻¹ or better. The Xe $5p^6-5p^56s$ line at 68,045 cm⁻¹ was also included in this multi-spectrum fit to verify the frequency calibration of all spectra, and is referenced to a high-accuracy measurement [23] of a single Xe isotope. Simulations of natural abundance Xe, as present in our experiment, including typical isotope splittings [24] indicate that our use of a purified calibration standard introduces a negligible error of (approximately 0.002 cm⁻¹). The estimated uncertainty of the resulting absolute calibration is 0.03 cm⁻¹ ¹ and additional fitting uncertainties of measured line frequencies are estimated during the optimisation of the model spectra and vary between 0.001 and 0.01 cm⁻¹. Besides a room temperature very-high pressure spectrum, 400 hPa, was also recorded using a 9 cm long MgF₂ windowed cell that could be inserted into the beam, allowing the measurement of weak extra-lines at high column density. Line frequencies of the $^{12}C^{18}O$ A $^{1}\Pi$ – $X^{1}\Sigma^{+}(2, 0)$ band are reported in Table 1. The extra-lines observed in this band are listed in Table 2.

2.2. High-resolution VIS-FT emission spectroscopy (University of Rzeszów)

For recording spectra of the $B^1\Sigma^+$ – $A^1\Pi(0, 2)$ and $C^1\Sigma^+$ – $A^1\Pi(0, 2)$ bands of the $^{12}C^{18}O$ isotopologue, a previously-described [19] air-cooled hollow-cathode (HC) lamp was used. The cathode was equipped with a cylinder made of graphite. Isotopically enriched molecular oxygen $^{18}O_2$ (Sigma-Aldrich, 98.1% $^{18}O_2$) was admitted to the lamp at about 3 hPa, and emission spectra were recorded during a sustained discharge with a 780 V DC voltage applied to the electrodes and a 54 mA current through the gas. The 1100 ± 50 K temperature of the intra-cathode plasma is estimated from vibrational contours of the studied bands [19] and is sufficient to collisionally populate rotational levels of $B^1\Sigma^+(v=0)$ and $C^1\Sigma^+(v=0)$ levels up to J=39 and 35, respectively, which radiatively decay to $A^1\Pi(v=2)$. This rotational excitation is higher than in our previous studies in which a plasma temperature of 300 K was achieved and also results in increased Doppler-broadening, but only to about 0.015 cm $^{-1}$ FWHM (full-width-at-half-maximum). Some spectral lines of $^{12}C^{16}O$ are observed in the spectrum and originate from approximate 1.9% $^{16}O_2$ oxygen contamination of the gas sample used in the experiment.

The $B^1\Sigma^+$ – $A^1\Pi(0, 2)$ and $C^1\Sigma^+$ – $A^1\Pi(0, 2)$ bands of $^{12}C^{18}O$ were recorded in a 128-scan acquisition of the 1.71-m Bruker (IFS 125-HR) spectrometer at the University of Rzeszów operating under vacuum condition (p < 0.01 hPa). The instrumental resolution is 0.018 cm $^{-1}$ and the obtained signal-to-noise ratio (SNR) for the recorded $B^1\Sigma^+$ – $A^1\Pi(0, 2)$ and $C^1\Sigma^+$ – $A^1\Pi(0, 2)$ bands is 90:1 and 20:1, respectively. A calibration of the frequency axis is performed with reference to the 633 nm He-Ne line produced by an internally stabilized laser (\pm 1.5 MHz/2h) and the calibration uncertainty (1σ) is estimated to be 0.004 cm $^{-1}$. The $B^1\Sigma^+$ – $A^1\Pi(0, 2)$ and $C^1\Sigma^+$ – $A^1\Pi(0, 2)$ spectra appear between 19,200 and 20,100 cm $^{-1}$, and 24,200 and 24,950 cm $^{-1}$, respectively, and are presented in Figs. 2 and 3 together with PGOPHER [25] simulations obtained from the final deperturbation analysis.

Voigt profiles were fitted to the observed line contours when reducing the spectrum to a list of transition frequencies, and their absolute accuracies are estimated to fall in the ranges 0.005-0.01 and 0.01-0.02 cm⁻¹ for the $B^1\Sigma^+-A^1\Pi(0,\ 2)$ and $C^1\Sigma^+-A^1\Pi(0,\ 2)$ bands, respectively, and depend on individual line intensities and degree of blending. The transition frequencies of lines in the $B^1\Sigma^+-A^1\Pi(0,\ 2)$ and $C^1\Sigma^+-A^1\Pi(0,\ 2)$ bands are listed in Tables 3 and 4, and for lines originating from $B^1\Sigma^+(v=0)$ and $C^1\Sigma^+(v=0)$ and associated with perturber states, i.e. $e^3\Sigma^-(v=4)$, $d^3\Delta(v=7)$ and $I^1\Sigma^-(v=3)$, are presented in Table 5.

The line list of the transition frequencies transitions and oscillator strengths, obtained in the VIS-FT and VUV-FT experiments and included into the deperturbation analysis, is provided in the Supplementary Material.

3. Deperturbation analysis

The $A^1\Pi$ state of CO exhibits a remarkably complicated rotational structures [1]. It results from multiple perturbations, mainly due to direct spin-orbit and rotation-electronic (*L*-uncoupling) interactions with both near and distant states. In addition, the $A^1\Pi$ state is perturbed indirectly by the $a^3\Pi$ state through spin-orbit, spin-electronic and rotation-electronic interactions mediated by the direct perturbers of $A^1\Pi$ [15,19]. The direct $a^3\Pi \sim A^1\Pi$ (spin-orbit) interaction exists as well but is negligible due to a small overlap integral between these states in the vibrational region under investigation.

A development version of the PGOPHER program [25,26] is used to identify perturbers of the $A^1\Pi(v=2)$ level and to carry out a deperturbation analysis based on an effective Hamiltonian (for matrix elements and other details see Supplementary Material). Initially, a model of ro-vibronic energy levels was built based on literature data [6,8,22,27–36] and permitted the identification of possible perturbers of $A^1\Pi(v=2)$ from a perturbation diagram, plotted in Fig. 4, as was also done in Refs. [13–15,19].

The B¹ $\Sigma^+(v=0)$ and C¹ $\Sigma^+(v=0)$ levels were represented in the model by the terms. This procedure, called the *term-value fitting approach*, eliminates the influence of the unidentified perturbations occurring in these levels [14,15,18,37–39] (see also Fig. 5 in Ref. [19]) on the deperturbation analysis of A¹ $\Pi(v=2)$. The term-values of B¹ $\Sigma^+(v=0)$ and C¹ $\Sigma^+(v=0)$ were fixed to fitted values obtained by Malicka et al. [19]. A detailed discussion of this approach within a dedicated least-squares method has been provided in Refs. [40–43]. The method allowed us to test the significance of thirty possible direct and indirect interactions potentially affecting the A¹ $\Pi(v=2)$ level, with results listed in Table 6. Term values of the X¹ $\Sigma^+(v=0)$ reference level were fixed to the values given by Coxon et al. [22].

High-accuracy data for 541 transitions from 5 bands: (i) $B^1\Sigma^+ - A^1\Pi(0, 2)$ and $C^1\Sigma^+ - A^1\Pi(0, 2)$ obtained by VIS-FT spectroscopy, and (ii) $A^1\Pi - X^1\Sigma^+(2, 0)$, $B^1\Sigma^+ - X^1\Sigma^+(0, 0)$, $C^1\Sigma^+ - X^1\Sigma^+(0, 0)$, obtained by VUV-FT spectroscopy, are used in the deperturbation analysis of $A^1\Pi(v=2)$. As a result, 17 independent parameters were obtained: 11 deperturbed molecular constants for the $A^1\Pi(v=2)$, $e^3\Sigma^-(v=4)$, $d^3\Delta(v=7)$, $a^{\prime 3}\Sigma^+(v=12)$ and $I^1\Sigma^-(v=3)$ levels; 3 spin-orbit coupling parameters describing the $A^1\Pi(v=2) \sim e^3\Sigma^-(v=4)$, $d^3\Delta(v=7)$ and $a^{\prime 3}\Sigma^+(v=12)$ perturbations as well as 3 rotation-electronic (*L*-uncoupling) interactions parameters parameterizing the $A^1\Pi(v=2) \sim I^1\Sigma^-(v=3)$, $I^1\Sigma^-(v=4)$ and $D^1\Delta(v=3)$ perturbations. The *L*-uncoupling interactions are parameterised with the symbol ξ , while the spin-orbit couplings are parameterized with the use of η [13,14,19]. The obtained parameters are presented in Table 7 and compared with analogous values determined by Beaty et al. [17] and Haridass et al. [16]. Ro-vibronic term values for $A^1\Pi(v=2)$, $e^3\Sigma^-(v=4)$, $d^3\Delta(v=7)$, $a^{\prime 3}\Sigma^+(v=12)$ and $I^1\Sigma^-(v=3)$ levels are listed in Table 8, while reduced terms are presented in Fig. 5.

At each stage of model fitting, the correlations between parameters were monitored. The final model reproduces the experimental data very well and the root-mean-square error (RMSE) of unweighted residuals for all transition frequencies amounts to 0.012 cm⁻¹. All details of the final

deperturbation analysis can be found in the PGOPHER file attached as Supplementary Material.

Perturbed line strengths of the $A^1\Pi - X^1\Sigma^+(2,0)$ transition and forbidden lines are calculated with the PGOPHER program and provide a check on the energy levels used to constrain the deperturbation model. Fig. 6 directly compares an experimental spectrum with a simulation from model line frequencies and strengths, which shows good agreement for both $A^1\Pi - X^1\Sigma^+(2,0)$ and forbidden transitions.

An alternative view of intra-molecular interactions is obtained through analysis of "borrowing" of $A^1\Pi$ character by the perturbing ro-vibrational levels. The admixture of ${}^1\Pi$ character as a percentage $C_{ik}^2 \cdot 100$, where $C_{ik} = \langle \Phi_k | \Psi_i \rangle$ is a mixing coefficient obtained from the eigenvectors of the diagonalised energy matrix in the final fit, which are presented in Fig. 7. The indirect interaction of the $a^3\Pi$ and $A^1\Pi$ states, identified here in ${}^{12}C^{18}O$, leads to a borrowing of ${}^3\Pi$ character in ${}^1\Pi$ and vice versa, as illustrated in Fig. 7.

4. Discussion

Beaty et al. [17] considered only two kinds of direct rotational perturbation in their analysis of the A¹ $\Pi(v=2)$ level: caused by an *L*-uncoupling interaction with I¹ $\Sigma^-(v=3)$ and the spin-orbit interaction with e³ $\Sigma^-(v=4)$. In turn, Haridass et al. [16], in their deperturbation analysis of A¹ $\Pi(v=2)$, considered 7 direct rotational perturbations caused by the A¹ $\Pi(v=2) \sim [I^1\Sigma^-(v=3), D^1\Delta(v=3)]$ *L*-uncoupling interactions and the A¹ $\Pi(v=2) \sim [e^3\Sigma^-(v=4), d^3\Delta(v=7, 8), a^{t^3}\Sigma^+(v=11, 12)]$ spin-orbit interactions. In this work the direct and indirect influences of 30 inter-electronic state interactions that potentially affect the A¹ $\Pi(v=2)$ level (based on Fig. 4) were examined (Table 6) and 16 significant interactions were included in a final deperturbation. Among them, a significant indirect influence of a³ Π on A¹ Π was detected in ¹²C¹⁸O: the a³ $\Pi(v=13) \sim [e^3\Sigma^-(v=4), d^3\Delta(v=7), a^{t^3}\Sigma^+(v=12)] \sim A^1\Pi(v=2)$ spin-orbit/spin-electronic/*L*-uncoupling and spin-orbit interactions as well as the a³ $\Pi(v=13) \sim [D^1\Delta(v=3), I^1\Sigma^-(v=3)] \sim A^1\Pi(v=2)$ spin-orbit and *L*-uncoupling interactions.

The indirect $a^3\Pi \sim A^1\Pi$ interaction in CO may lead to a metastable population following $A^1\Pi \leftarrow X^1\Sigma^+$ pumping. The $a^3\Pi - X^1\Sigma^+$ transition borrows strength only from the $A^1\Pi - X^1\Sigma^+$ transition, and essentially only from $A^1\Pi(v=2) - X^1\Sigma^+$. The absorption strength of specific rotational transitions is proportional to their fractional ${}^1\Pi$ character, shown in Fig. 7, at most 0.6%. The intensity of optically-forbidden transitions to perturbed $a^3\Pi$ levels are then a factor of $10^3 - 10^4$ weaker than corresponding transitions to $A^1\Pi$ and the indirect $a^3\Pi(v=13) \sim A^1\Pi(v=2)$ interaction is not detectable by the observation of level shifts or intensity anomalies. Instead, it relies on a precise fit of multiple direct perturbations that is taken here to a new level. Even a weak indirect $a^3\Pi \sim A^1\Pi$ interaction might provide a method for excitation of a single vibration-rotation-fine-structure level of

 $a^3\Pi$, or lead to a high fluorescence quenching rate for the most-affected levels of $A^1\Pi$. Such a collisional effect also raises the possibility of anomalously state-selective chemistry.

The borrowing of $A^1\Pi(v=2)$ percentage character by perturbing levels is shown in Fig. 7. The $A^1\Pi(v=2) \sim d^3\Delta(v=7)$ interaction causes a decrease in the $^1\Pi$ character of $A^1\Pi(v=2)$, by more than 50% for both the F_{1f} component at J=40 and F_{1e} component at J=33. The responsible perturbing levels are the F_{1f} (3% $^1\Pi$), F_{2f} (16% $^1\Pi$), F_{3f} (22% $^1\Pi$), F_{1e} (24% $^1\Pi$), F_2 .(19% $^1\Pi$) F_{3e} (5% $^1\Pi$) sublevels of $d^3\Delta(v=7)$. The largest $^1\Pi$ character borrowing is by the F_{2f} component of $e^3\Sigma^-(v=4)$ (39 at J=28). The most significant contribution to the borrowing of $^1\Pi$ character is due to the direct spin-orbit perturbations. These perturbations also lead to the largest term-value perturbations at anticrossings of $A^1\Pi(v=2)$ with $d^3\Delta(v=7)$, $e^3\Sigma^-(v=4)$, and $a'^3\Sigma^+(v=12)$ (see Fig. 5). An interesting case is that of the e and f components of $D^1\Delta(v=3)$ which take on a relatively large amount of $^1\Pi$ character (even 9% for J=48), similar to the $a'^3\Sigma^+(v=12)$ level (8 - 9% for J=42), even though the $A^1\Pi\sim D^1\Delta$ interaction has rotation-electronic nature. The explanation is that the heterogeneous rotation-electronic interaction depends strongly on the quantum number J, which is quite high in this case.

Fig. 7 also shows that the $a^3\Pi(v=13)$ level acquires a small part of the ${}^1\Pi$ percentage character ($\sim 0.02\%$). However, this occurs only and exclusively because of the mediation of the $e^3\Sigma^-(v=4)$, $d^3\Delta(v=7)$, $a'^3\Sigma^+(v=12)$ and $D^1\Delta(v=3)$ levels between the $A^1\Pi(v=2)$ and $a^3\Pi(v=13)$ interactions. The direct influence of $a^3\Pi(v=13)$ is negligibly small due to extremely small vibrational overlap integral $\langle v_{A(2)}|v_{a(13)}\rangle=1.22\times10^{-4}$. The borrowing of this $a^3\Pi(v=13)$ state character is visible only near in the locations of the strongest interactions of the $a^3\Pi(v=13)$ state with the $e^3\Sigma^-(v=4)$, $d^3\Delta(v=7)$, $a'^3\Sigma^+(v=12)$ and $D^1\Delta(v=3)$ levels (see the lowest plot of Fig. 7): $a^3\Pi(v=13,F_{1e},F_{2e})\sim e^3\Sigma^-(v=4,F_{1e},F_{3e})$ for J=25, $a^3\Pi(v=13,F_{1e},F_{2e})\sim e^3\Sigma^-(v=4,F_{1e},F_{3e})$ for J=31; $a^3\Pi(v=13)\sim d^3\Delta(v=7)$ for J=33, 36, 40 (all components); $a^3\Pi(v=13,F_{1e},F_{2e},F_{3e})\sim a'^3\Sigma^+(v=12,F_{3e})$ for J=39; $a^3\Pi(v=13,F_{1e},F_{2e})\sim a'^3\Sigma^+(v=12,F_{3f})$ for J=37 and 42; $a^3\Pi(v=13)\sim D^1\Delta(v=3)$ for J=48 (all components).

High precision, deperturbed molecular constants for $A^1\Pi(v=2)$, $e^3\Sigma^-(v=4)$, $d^3\Delta(v=7)$, $a'^3\Sigma^+(v=12)$, $D^1\Delta(v=3)$ and $I^1\Sigma^-(v=3,4)$ are listed in Table 7 and compared with analogous values determined by Beaty et al. [17] and Haridass et al. [16]. This comparison is limited with regard to T and B constants because the authors of Ref. [16,17] define their effective Hamiltonian in terms of rotational angular-momentum of the nuclear framework (operator \hat{R}), whilst in this work an operator describing the total angular momentum excluding spin (\hat{N}) was implemented in accordance with IUPAC recommendations [44]. Details about this issue are presented in Ref. [19]. All the molecular constants determined in this work are estimated to be one to three orders-of-magnitude more precise than previously known.

The parameters describing $A^1\Pi(v=2) \sim [e^3\Sigma^-(v=4), d^3\Delta(v=7), a'^3\Sigma^+(v=12)]$ spin-orbit interactions listed in Table 7 are in very good agreement with both calculated values (relative error no

larger than 1.6) and previous experimental estimates in Refs. [16,17] (but with two to three orders-of-magnitude improved precision). The calculated values were obtained within this work on the basis of isotopologue-independent purely electronic $a_{A\sim d,e,a'}$ and $b_{A\sim D,I}$ parameters (given by Hakalla et al. [13] for $A^1\Pi \sim a'$ and $A^1\Pi \sim D$ interactions as well as obtained using data from Le Floch et al. [8] for $A^1\Pi \sim [e^3\Sigma^-, d^3\Delta$ and $I^1\Sigma^-]$ perturbations) based on the Eqns.(1) - (5) from Hakalla et al. [13] and Eqns.(1) - (3) from Malicka et al. [19]. A way to obtain the vibrational overlap integrals $\langle v_A|v_{a',e,d}\rangle$ and rotational operator integrals $\langle v_A|\widehat{B(R)}|v_{I,D}\rangle$ is highlighted in Refs. [13,14].

The relative errors expressed as percentage difference between theoretical and fitted values of the $A^1\Pi(v=2)\sim [I^1\Sigma^-(v=3),\ D^1\Delta(v=3)]$ and $I^1\Sigma^-(v=4)$ rotation-electron (*L*-uncoupling type) perturbation parameters (6.5 , 20.2 , 21.6 , respectively) are greater than the other fitted ones and listed in Table 7. The reasons are that: (i) all of these interactions are strongly *J*-dependent and the $A^1\Pi(v=2)\sim I^1\Sigma^-(v=3)$ perturbation falls on J=7-8; (ii) the $A^1\Pi(v=2)\sim [D^1\Delta(v=3)]$ and $I^1\Sigma^-(v=4)$] perturbations affect $A^1\Pi(v=2)$ most strongly at J=48 and 53 – 54, respectively, which is almost out of the experimental range of the present work. Our results are still significantly more accurate than found by Refs. [16,17] for these parameters.

Tables 1, 3 and 4 show the measured frequencies of $A^1\Pi - X^1\Sigma^+(2, 0)$, $B^1\Sigma^+ - A^1\Pi(0, 2)$ and $C^1\Sigma^+ - A^1\Pi(0, 2)$ bands. Some low-intensity lines associated with higher rotational levels J = 31 - 33 and 40 - 48 of the $A^1\Pi(v = 2)$ level are marked with an asterisk in these Tables and are not included in the final deperturbation. This was necessary because a significant indirect influence of $a^3\Pi(v = 13)$ on $A^1\Pi(v = 2)$ is evident but is unconstrained because of: (i) a lack of extra-lines connected to $a^3\Pi(v = 13)$ apparent in our spectra that require the molecular constants of $a^3\Pi(v = 13)$ to be fixed to mass scaled values that are usually insufficiently accurate for a spectroscopically-accurate deperturbation; (ii) independently fitting the $a^3\Pi(v = 13) \sim [e^3\Sigma^-(v = 4), d^3\Delta(v = 7), a'^3\Sigma^+(v = 12)]$ interactions is statistically unjustified and leads to strong correlations with other model parameters, but neglecting these entirely degrades the final fit and these parameters are then fixed to values calculated in this work (see Table 7) for details); (iii) the spin-spin $d^3\Delta(v = 7) \sim [e^3\Sigma^-(v = 4), a'^3\Sigma^+(v = 12)]$ and spin-orbit $e^3\Sigma^-(v = 4) \sim a'^3\Sigma^+(v = 12)$ interactions are fixed to zero because fitting them is statistically unjustified or leads to strong correlations with other model parameters (see Table 6) and their theoretical values are unknown.

Fig. 5 shows reduced term values of $A^1\Pi(v=2)$ and its perturbers. The largest shift of perturbed $A^1\Pi(v=2)$ energy levels (approx. 5.5 cm⁻¹) occurs for the F_{1f} level at J=28 and it is due to the $A^1\Pi(v=2) \sim e^3\Sigma^-(v=4)$ spin-orbit interaction. In comparison, the $A^1\Pi(v=2) \sim I^1\Sigma^-(v=3)$ perturbation, the maximum of which falls at J=8, is quite interesting because both have a similar value of the overlap integrals $(\langle v_{A(2)}|v_{e(4)}\rangle = -0.2994, \langle v_{A(2)}|\widehat{\boldsymbol{B}(\boldsymbol{R})}|v_{I(3)}\rangle = 0.3301 \text{ cm}^{-1})$ and similar distances of unperturbed terms (about 3 cm⁻¹), but the $A^1\Pi(v=2) \sim I^1\Sigma^-(v=3)$ interaction is over 50 times weaker. Such behaviour is the result of the J-dependent nature of the interaction. For this reason,

among the observed rotation-electronic interactions, a three times greater term value shift (approx. 0.3 cm⁻¹) occurs for the $A^1\Pi(v=2) \sim D^1\Delta(v=3)$ interaction. It is associated with a higher rotational level (J=48), even though the value of the overlap integral is slightly smaller $(\langle v_{A(2)} | \widehat{\boldsymbol{B}(\boldsymbol{R})} | v_{D(3)} \rangle = 0.2628$ cm⁻¹), and the minimum energy separation between unperturbed levels is larger (approx. 6 cm⁻¹) compared to the $A^1\Pi(v=2)$ and $I^1\Sigma^-(v=3)$ levels (approx. 3 cm⁻¹). The second-largest shifts in terms of the $A^1\Pi(v=2)$ level, approx. 4.2 cm⁻¹, are caused by spin-orbit interactions with the $d^3\Delta(v=7, F_{3e_3})$ components and their maxima are located at J=40.

5. Conclusions

Using two Fourier-transform spectroscopic techniques (in combination with synchrotron radiation absorption and discharge emission) high-resolution measurements of three $^{12}C^{18}O$ bands were performed: $A^1\Pi - X^1\Sigma^+(2,0)$, $B^1\Sigma^+ - A^1\Pi(0,2)$ and $C^1\Sigma^+ - A^1\Pi(0,2)$. The frequency accuracies amounted to about 0.01, 0.005 and 0.01 cm $^{-1}$, respectively. Transitions forbidden by spin- and electric-dipole selection rules are also observed arising from spin-orbit and rotation-electronic interactions of $e^3\Sigma^-(v=4)$, $d^3\Delta(v=7)$, $a'^3\Sigma^+(v=12)$ and $I^1\Sigma^-(v=3)$ with $A^1\Pi(v=2)$. All new experimental data, and additional VUV-FT data for $^{12}C^{18}O$ $B^1\Sigma^+ - X^1\Sigma^+(0,0)$ and $C^1\Sigma^+ - X^1\Sigma^+(0,0)$ bands [19] (a total of 541 line frequencies) is included in a deperturbation analysis of $A^1\Pi(v=2)$.

Finally, 11 deperturbed molecular constants and 6 interaction energies were obtained, along with 110 experimental ro-vibrational term values of $A^1\Pi(\nu=2)$ and perturbing $e^3\Sigma^-(\nu=4)$, $I^1\Sigma^-(\nu=3)$, $a'^3\Sigma^+(\nu=12)$, $d^3\Delta(\nu=7)$ levels. An statistically significant, indirect influence of $a^3\Pi$ on the $A^1\Pi$ state was detected for the first time in $^{12}C^{18}O$. It occurs via simultaneous spin-orbit, spin-electronic and rotation-electronic interactions: $a^3\Pi(\nu=13) \sim [e^3\Sigma^-(\nu=4), \ d^3\Delta(\nu=7), \ a'^3\Sigma^+(\nu=12)] \sim A^1\Pi(\nu=2)$ and $a^3\Pi(\nu=13) \sim [D^1\Delta(\nu=3), \ I^1\Sigma^-(\nu=3)] \sim A^1\Pi(\nu=2)$. It is uniquely observed in the $^{12}C^{18}O$ isotopologue under present consideration because of the high precision of the observations and the careful characterization of all direct interactions with the $A^1\Pi(\nu=2)$ and $a^3\Pi(\nu=13)$ level. With the inclusion of this large number of interacting states, the present case of both $A^1\Pi(\nu=2)$ and $a^3\Pi(\nu=13)$ states with an in-common group of perturbing states ranks among the most complete deperturbation analyses of interacting states in diatomic molecules. As such it is exemplary for the depth to which perturbation analyses can be performed. The new results provide a significantly improved description of the $A^1\Pi(\nu=2)$ and $a^3\Pi(\nu=13)$ levels in $^{12}C^{18}O$ and their complex web of intra-molecular interactions.

Acknowledgments

RH is indebted to Professor Colin M. Western (University of Bristol) for his enormous help with implementing *the term-value fitting approach* method into the development version of the PGOPHER code and for a lot of valuable discussions. RH thanks LASERLAB-EUROPE for support of this research [grants: EUH2020-RIP-654148 and EC's-SPF-284464] as well as European Regional

Development Fund and the Polish state budget within the framework of the Carpathian Regional Operational Programme [grant number RPPK.01.03.00-18-001/10] through the funding of the Centre for Innovation and Transfer of Natural Sciences and Engineering Knowledge of the University of Rzeszów. AH acknowledges grant funding from the CAAS ERDF/ESF "Centre of Advanced Applied Sciences" (No. CZ.02.1.01/0.0/0.0/16_019/0000778). R.W. Field thanks the US National Science Foundation (grant number CHE-1800410) for support of his research, which includes substantial collaborations. The authors are grateful to the general and technical staff of SOLEIL synchrotron for running the facility and providing beam time under project numbers 20120653 and 20160118.

References

- [1] Lefebvre-Brion H, Field RW. The spectra and dynamics of diatomic molecules. Amsterdam: The Netherlands: Elsevier Academic Press; 2004.
- [2] Hall JA, Schamps J, Robbe JM, Lefebvre-Brion H. Theoretical study of perturbation parameters in the a³Π and a A¹Π states of CO. Journal of Chemical Physics 1973;59:3271–83. https://doi.org/10.1063/1.1680469.
- [3] Dame TM, Hartmann D, Thaddeus P. The milky way in molecular clouds: A new complete CO survey. Astrophysical Journal 2001;547:792–813. https://doi.org/10.1086/318388.
- [4] Kong S, Lada CJ, Lada EA, Román-Zúñiga C, Bieging JH, Lombardi M, et al. The relationship between the dust and gas-phase CO across the california molecular cloud. The Astrophysical Journal 2015;805:58. https://doi.org/10.1088/0004-637X/805/1/58.
- [5] Sheffer Y, Federman SR, Lambert DL, Cardelli JA. Fractionation of CO in the diffuse clouds toward zeta ophiuchi. Astrophysical Journal 1992;397:482–91. https://doi.org/10.1086/171805.
- [6] Field RW. Spectroscopy and perturbation analysis in excited states of CO and CS. PhD thesis. Harvard University; 1971.
- [7] Field RW, Simmons JD, Tilford SG, Wicke BG. Analysis of perturbations in a³Π and A¹Π states of CO. Journal of Molecular Spectroscopy 1972;44:383–99. https://doi.org/10.1016/0022-2852(72)90111-7.
- [8] Le Floch AC, Launay F, Rostas J, Field RW, Brown CM, Yoshino K. Reinvestigation of the CO A¹Π state and its perturbations the v=0 levels. Journal of Molecular Spectroscopy 1987;121:337–79. https://doi.org/10.1016/0022-2852(87)90056-7.
- [9] Le Floch AC, Rostas J, Schamps J. The A¹Π ~ D ¹Δ rotation-electronic interaction in CO. Molecular Physics 1988;63:677–84.
- [10] Le Floch AC. Ph.D. thesis. University Paris-Sud, Orsay 1989.
- [11] Niu ML, Salumbides EJ, Zhao D, de Oliveira N, Joyeux D, Nahon L, et al. High resolution spectroscopy and perturbation analysis of the CO $A^1\Pi X^1\Sigma^+$ (0,0) and (1,0) bands. Molecular Physics 2013;111:2163–74. https://doi.org/10.1080/00268976.2013.793889.
- [12] Niu ML, Hakalla R, Trivikram TM, Heays AN, de Oliveira N, Salumbides EJ, et al. Spectroscopy and perturbation analysis of the $A^1\Pi$ (ν =0) state of $^{13}C^{16}O$. Molecular Physics 2016;114:2857–67. https://doi.org/10.1080/00268976.2016.1218078.
- [13] Hakalla R, Niu ML, Field RW, Salumbides EJ, Heays AN, Stark G, et al. VIS and VUV spectroscopy of ¹²C¹⁷O and deperturbation analysis of the A¹Π, v = 1–5 levels. Royal Society of Chemistry Advances 2016;6:31588–606. https://doi.org/10.1039/C6RA01358A.
- [14] Hakalla R, Niu ML, Field RW, Heays AN, Salumbides EJ, Stark G, et al. Fourier-transform spectroscopy of ¹³C¹⁷O and deperturbation analysis of the A¹Π (*ν*=0–3) levels. Journal of Quantitative Spectroscopy and Radiative Transfer 2017;189:312–28. https://doi.org/10.1016/j.jqsrt.2016.12.012.
- [15] Hakalla R, Trivikram TM, Heays AN, Salumbides EJ, de Oliveira N, Field RW, et al. Precision spectroscopy and comprehensive analysis of perturbations in the $A^1\Pi(\nu=0)$ state of $^{13}C^{18}O$. Molecular Physics 2019;117:79–96. https://doi.org/10.1080/00268976.2018.1495848.

- [16] Haridass C, Reddy SP, Le Floch AC. The 4th Positive $A^1\Pi X^1\Sigma^+$ System of $^{12}C^{18}O$ and $^{13}C^{18}O$: Perturbations in the $A^1\Pi$ State. Journal of Molecular Spectroscopy 1994;167:334–52. https://doi.org/10.1006/jmsp.1994.1240.
- [17] Beaty LM, Braun VD, Huber KP, Le Floch AC. A high-resolution 18 O isotope study in the vacuum ultraviolet of the $A^1\Pi$ $X^1\Sigma^+$ 4th positive system of CO. Astrophysical Journal Supplement Series 1997;109:269–77. https://doi.org/10.1086/312976.
- [18] Trivikram TM, Hakalla R, Heays AN, Niu ML, Scheidegger S, Salumbides EJ, et al. Perturbations in the A $^{1}\Pi$, v = 0 state of $^{12}C^{18}O$ investigated via complementary spectroscopic techniques. Molecular Physics 2017;115:3178–91. https://doi.org/10.1080/00268976.2017.1356477.
- [19] Malicka MI, Ryzner S, Heays AN, de Oliveira N, Field RW, Ubachs W, et al. High-resolution Fourier-transform spectroscopy and deperturbation analysis of the $A^1\Pi(\nu=1)$ level in $^{12}C^{18}O$. Journal of Quantitative Spectroscopy and Radiative Transfer 2020;255:107243. https://doi.org/10.1016/j.jqsrt.2020.107243.
- [20] de Oliveira N, Roudjane M, Joyeux D, Phalippou D. High-resolution broad-bandwidth Fourier-transform absorption spectroscopy in the VUV range down to 40 nm. Nature Photonics 2011;5:149–53. https://doi.org/10.1038/NPHOTON.2010.314.
- [21] de Oliveira N, Joyeux D, Roudjane M, Gil J-F, Pilette B, Archer L, et al. The high-resolution absorption spectroscopy branch on the VUV beamline DESIRS at SOLEIL. Journal of Synchrotron Radiation 2016;23:887–900. https://doi.org/10.1107/S1600577516006135.
- [22] Coxon JA, Hajigeorgiou PG. Direct potential fit analysis of the $X^1\Sigma^+$ ground state of CO. Journal of Chemical Physics 2004;121:2992–3008. https://doi.org/10.1063/1.1768167.
- [23] Ozawa A, Kobayashi Y. VUV frequency-comb spectroscopy of atomic xenon. Physical Review A 2013;87:022507. https://doi.org/10.1103/PhysRevA.87.022507.
- [24] Brandi F, Velchev I, Hogervorst W, Ubachs W. Vacuum-ultraviolet spectroscopy of Xe: Hyperfine splittings, isotope shifts, and isotope-dependent ionization energies. Physical Review A 2001;64:032505. https://doi.org/10.1103/PhysRevA.64.032505.
- [25] Western C. PGOPHER: a program for simulating rotational structure. Development version. University of Bristol, Bristol, Http://Pgopher.Chm.Bris.Ac.Uk/: 2020.
- [26] Western C. PGOPHER: A program for simulating rotational, vibrational and electronic spectra. Journal of Quantitative Spectroscopy and Radiative Transfer 2017;186:221-42. https://doi.org/10.1016/j.jqsrt.2016.04.010.
- [27] Kępa R, Ostrowska-Kopeć M, Piotrowska I, Zachwieja M, Hakalla R, Szajna W, et al. Ångström $(B^1\Sigma^+ \to A^1\Pi)$ 0-1 and 1-1 bands in isotopic CO molecules: further investigations. Journal of Physics B: Atomic, Molecular and Optical Physics 2014;47:045101. https://doi.org/10.1088/0953-4075/47/4/045101.
- [28] Eidelsberg M, Roncin JY, Le Floch AC, Launay F, Letzelter C, Rostas J. Reinvestigation of the vacuum ultraviolet-spectrum of CO and isotopic-species $B^1\Sigma^+ \leftrightarrow X^1\Sigma^+$ transition. Journal of Molecular Spectroscopy 1987;121:309–36. https://doi.org/10.1016/0022-2852(87)90055-5.
- [29] Ubachs W, Hinnen PC, Hansen P, Stolte S, Hogervorst W, Cacciani P. Laser spectroscopic studies of the $C^1\Sigma^+$, $(\nu=0)$ and $(\nu=1)$ states of CO. Journal of Molecular Spectroscopy 1995;174:388–96. https://doi.org/10.1006/jmsp.1995.0010.
- [30] Tilford SG, Howard RA, Ginter ML. Fluorescence of carbon-monoxide excited by 1306-Å oxygen resonance line. Journal of Chemical Physics 1972;56:1413–5. https://doi.org/10.1063/1.1677380.
- [31] Kittrell C, Garetz BA. Analysis of the $D^1\Delta$ $X^1\Sigma^+$ transition in CO observed by two-photon excitation. Spectrochim Acta Part A-Molecular and Biomolecular Spectroscopy 1989;45:31–40. https://doi.org/10.1016/0584-8539(89)80024-8.
- [32] Wolk GL, Rich JW. Observation of a new electronic state of carbon-monoxide using LIF on highly vibrationally excited CO ($X^1\Sigma^+$). Journal of Chemical Physics 1983;79:12–8. https://doi.org/10.1063/1.445571.
- [33] Vazquez GJ, Amero JM, Liebermann HP, Lefebvre-Brion H. Potential Energy Curves for the $^1\Sigma^+$ and $^{1,3}\Pi$ States of CO. Journal of Physical Chemistry A 2009;113:13395–401. https://doi.org/10.1021/jp902730d.

- [34] Kępa R. New spectroscopic studies of the Herzberg bands of the ¹²C¹⁶O molecule. Journal of Molecular Spectroscopy 1989;135:119–30. https://doi.org/10.1016/0022-2852(89)90359-7.
- [35] Huber KP, Herzberg G. Constants of diatomic molecules. New York: Nostrand Reinhold; 1979.
- [36] Rytel T. Analysis of the Perturbed 2-2 Band of the Third Positive ($b^3\Sigma^+$ $a^3\Pi_r$) System of CO. Journal of Molecular Spectroscopy 1992;151:271–4.
- [37] Janjić J, Danielak J, Kępa R, Rytel M. The Ångström bands of ¹³C¹⁶O and ¹²C¹⁸O molecules. Acta Physica Polonica A 1972:41:757-61.
- [38] Lemaire JL, Heays AN, Eidelsberg M, Gavilan L, Stark G, Federman SR, et al. Atlas of new and revised high-resolution spectroscopy of six CO isotopologues in the 101-115nm range. Transition energies of the v'=0, 1, 2, and 3 to v"=0 bands of the $B^1\Sigma^+$, $C^1\Sigma^+$, and $E^1\Pi$ to $X^1\Sigma^+$ states, related term values, and molecular constants. Astronomy & Astrophysics 2018;614:A114. https://doi.org/10.1051/0004-6361/201732114.
- [39] Amiot C, Roncin JY, Verges J. First observation of the CO $E^1\Pi$ to $B^1\Sigma^+$ and $C^1\Sigma^+$ to $B^1\Sigma^+$ band systems. Predissociation in the $E^1\Pi(\nu=0)$ level. Journal of Physics B: Atomic and Molecular Physics 1986;19:L19–23. https://doi.org/10.1088/0022-3700/19/1/004.
- [40] Åslund N. Numerical-method for simultaneous determination of term values and molecular-constants. Journal of Molecular Spectroscopy 1974;50:424–34. https://doi.org/10.1016/0022-2852(74)90245-8.
- [41] Curl RF, Dane CB. Unbiased least-squares fitting of lower states. Journal of Molecular Spectroscopy 1988;128:406-12. https://doi.org/10.1016/0022-2852(88)90157-9.
- [42] Watson JKG. On the use of term values in the least-squares fitting of spectra. Journal of Molecular Spectroscopy 1989;138:302–8. https://doi.org/10.1016/0022-2852(89)90119-7.
- [43] Focsa C, Poclet A, Pinchemel B, Le Roy R, Bernath P. Fourier transform spectroscopy of the $A'^1\Pi X^1\Sigma^+$ system of CaO. Journal of Molecular Spectroscopy 2000;203:330–8. https://doi.org/10.1006/jmsp.2000.8187.
- [44] Hirota E, Brown J, Hougen J, Shida T, Hirota N. Symbols for fine and hyperfine-structure parameters. Pure and Applied Chemistry 1994;66:571–6. https://doi.org/10.1351/pac199466030571.
- [45] Niu ML, Salumbides EJ, Heays AN, de Oliveira N, Field RW, Ubachs W. Spectroscopy and perturbation analysis of the CO $A^1\Pi X^1\Sigma^+$ (2,0), (3,0) and (4,0) bands. Molecular Physics 2016;114:627–36. https://doi.org/10.1080/00268976.2015.1108472.
- [46] de Nijs AJ, Salumbides EJ, Eikema KSE, Ubachs W, Bethlem HL. UV-frequency metrology on CO (a³Π): Isotope effects and sensitivity to a variation of the proton-to-electron mass ratio. Physical Review A 2011;84:052509. https://doi.org/10.1103/PhysRevA.84.052509.
- [47] Field RW, Tilford SG, Simmons JD, Howard RA. Fine-structure and perturbation analysis of a³Π state of CO. Journal of Molecular Spectroscopy 1972;44:347–82. https://doi.org/10.1016/0022-2852(72)90110-5.
- [48] Yamamoto S, Saito S. The microwave spectra of CO in the electronically excited states ($a^3\Pi_r$ and $a^{'3}\Sigma^+$). Journal of Chemical Physics 1988;89:1936–44. https://doi.org/10.1063/1.455091.
- [49] Herzberg G, Simmons JD, Bass A, Tilford SG. Forbidden I¹Σ⁻ X¹Σ⁺ absorption bands of carbon monoxide. Canadian Journal of Physics 1966;44:3039–45. https://doi.org/10.1139/p66-249
- [50] Garetz BA, Kittrell C, Le Floch, AC. Analysis of the two-photon $D^1\Delta X^1\Sigma^+$ transition in CO: Perturbations in the (10–0) band. Journal of Chemical Physics 1991;94:843–53. https://doi.org/10.1063/1.459973.

TABLES

Table 1 Transition frequencies (in cm $^{-1}$) of the $A^1\Pi - X^1\Sigma^+(2,0)$ VUV-FT absorption band in $^{12}C^{18}O.^{a,b}$

J''	R(J'')	O-C	Q(J'')	O-C	P(J'')	0-с
0	67,618.07(3)	0.01	-	-	-	-
1	67,620.35(3)	0.02	67,614.41(3)	0.02	-	-
2	67,621.93(3)	0.02	67,613.02(3)	0.02	67,607.08(3)	0.01
3	67,622.83(3)	0.02	67,610.94(3)	0.01	67,602.04(3)	0.02
4	$67,623.02(3)^{b}$	0.02	67,608.16(3)	0.01	$67,596.30(3)^{b}$	0.02
5	$67,622.53(3)^{b}$	0.02	$67,604.70(3)^{b}$	0.02	67,589.88(3)	0.02
6	67,621.34(3) ^b	0.02	67,600.53(3)	0.02	67,582.75(3)	0.02
7	67,619.46(3)	0.02	67,595.58(3)	0.02	67,574.94(3)	0.02
8	67,616.88(3)	0.02	$67,590.33(3)^{b}$	0.02	67,566.43(3)	0.02
9	67,613.61(3)	0.02	67,584.01(3)	0.02	67,557.23(3)	0.02
10	67,609.64(3)	0.02	67,577.06(3)	0.03	67,547.34(3)	0.02
11	67,604.97(3)	0.02	67,569.43(3)	0.03	67,536.76(3)	0.02
12	67,599.61(3) ^b	0.03	67,561.11(3)	0.03	67,525.48(3)	0.02
13	67,593.55(3)	0.03	67,552.09(3)	0.03	67,513.51(3)	0.02
14	67,586.78(3)	0.03	67,542.37(3)	0.02	67,500.85(3)	0.03
15	67,579.32(3)	0.03	$67,531.97(3)^{b}$	0.03	67,487.49(3)	0.03
16	67,571.15(3)	0.03	67,520.86(3)	0.03	67,473.43(3)	0.03
17	67,562.28(3)	0.03	67,509.06(3)	0.03	67,458.67(3)	0.03
18	67,552.69(3)	0.03	67,496.54(3)	0.03	67,443.22(3)	0.03
19	67,542.39(3)	0.03	$67,483.33(3)^{b}$	0.02	67,427.07(3)	0.03
20	67,531.35(3)	0.02	67,469.42(3)	0.03	67,410.20(3)	0.03
21	67,519.54(3) ^b	0.02	67,454.79(3)	0.03	67,392.63(3)	0.03
22	67,506.85(3)	0.02	67,439.44(3)	0.03	67,374.32(3)	0.02
23		0.03	67,423.36(3)	0.03	67,355.25(3)	0.02
24	67,483.74(3)	0.02	67,406.52(3)	0.02	67,335.31(3)	0.02
25		0.01	67,388.88(3)	0.02	67,313.88(3)	0.03
26		0.01	67,370.27(3)	0.02	67,297.72(3)	0.02
27		0.01	67,350.01(3)	0.01	67,274.14(3)	0.01
28	67,418.73(3)	0.02	67,339.58(3)	0.02	67,251.26(3)	0.01
29		0.02	67,315.66(3)	0.02	67,227.88(3)	0.01
30		- 0	67,293.76(3)	0.02	67,203.81(3)	0.02
31	67,367.27(3)*		67,271.72(3)	0.01	67,178.83(3)	0.02
32		-	67,249.11(3)	0.01	67,151.97(3)*	-
33		0.01	67,224.66(3)*	-	67,130.77(3)*	-
34		-0.01	67,202.20(3)	0.01	67,101.33(3)*	_
35	67,282.28(3)	0.01	67,177.43(3)	-0.01	67,075.23(3)	0.01
	67,261.87(3)	0.02	67,151.28(3)	0.01	$67,046.81(3)^{b}$	-0.01
37		-0.01	67,128.13(3)	-0.01	67,017.12(3)	0.01
38	67,213.15(3)	-0.02	67,100.44(3)	-0.01	66,989.56(3)	0.02
39	67,193.79(3)*	_	67,072.62(3)	0.01	66,958.62(3)	-0.01
40		-0.01	67,048.41(3)*	-	66,926.58(3)	-0.02
	67,139.44(4)	-0.01	$67,016.79(3)^{b}$	-0.02	66,900.12(3)*	-
	67,112.66(4)	-0.01	66,986.07(4)*	-	66,864.97(3)	-0.01
	67,085.19(4)	-0.02	66,957.05(4)	0.01	66,831.58(4)	-0.01
	67,057.05(4)	0.01	66,925.96(4)	0.01	66,797.71(4)	-0.01
	67,028.16(4)	0.01	66,894.24(4)	0.01	66,763.18(4)	-0.02
	66,998.55(4)	0.03	66,861.81(4)	0.02	66,727.98(4)	0.01
47		-	-	-	66,692.06(4)	0.01
	66,937.32(4) ^w	0.02	_	_	66,655.41(4)	0.03
	66,905.47(4) ^w	0.03	_	_	66,617.91(4)*	-
50	, / (-)				66,580.15(4)	0.02
		1	1 cm ⁻¹ and combined fi	44:		

^a The instrumental resolution was $0.31~{\rm cm}^{-1}$ and combined fitting and calibration 1σ frequency uncertainties are given in parentheses in terms of the least-significant digit. The absolute calibration uncertainty is $0.03~{\rm cm}^{-1}$ and the fitting uncertainties are estimated to vary between 0.006 and $0.1~{\rm cm}^{-1}$, depending on the line intensity and blending. The "o-c" columns lists observed minus calculated frequencies.

^b Lines marked with *b* and/or *w* are blended and/or weak.

^{*} The lines marked with an asterisk were not used in the final fit.

- 16 -

J''	$^{q}Q_{11fe}$	0-с	${}^qR_{11ee}$	0-с	$^{o}P_{11ee}$	0-с	$^{q}Q_{21fe}$	0-с	$^{p}Q_{11fe}$	0-с	$^rQ_{31fe}$	0-с	$^{r}R_{21fe}$	о-с
							$I^1\Sigma^ X^1\Sigma^+$ (3,	0)						
7	67,598.35(4)	0.03												
8	67,587.19(4) ^b	0.03												
							$e^3\Sigma^ X^1\Sigma^+$ (4.	. 0)						
23			67,508.63(4) ^b	0.03										
24			67,471.01(4)	0.02										
25			67,438.70(4)	-0.01	67,329.85(3)	0.04	67,441.78(4)	0.02						
26			, , , ,		67,284.98(4)	0.02	, , ,							
27					67,245.43(4)	-0.01	67,371.42(3)	0.01						
28							67,324.11(4)	-0.03						
29							67,288.22(4)*	- 4						
							$d^3\Delta - X^1\hat{\Sigma}^+(7,$	0)						
32			67,348.21(4)	0.02										
33									67,227.94(4) ^b	-0.01				
34					67,104.54(4)	0.03								
							$a^{\prime 3}\Sigma^+ - X^1\Sigma^+$ (1	2, 0)						
41														
42							. [//]				66,992.31(5)	0.03		
44													66,863.84(5) ^w	0.04

 ⁴⁴ a The uncertainties in parentheses indicate 1σ standard deviations and are a combination of fitting and calibration errors.
 b Lines marked with b and/or w are blended and/or weak.
 c The superscripts o, p, q, r and s denote change in the total angular momentum excluding spin.
 * The lines marked with an asterisk were not used in the final fit.

Table 3 Transition frequencies (in cm⁻¹) of the $B^1\Sigma^+ - A^1\Pi(0, 2)$ VIS-FT emission band in $^{12}C^{18}O.^{a,b}$

.J"	R(J'')	o-c	O(J'')	0-с	P(J'')	0-с
1	19,309.74(2) ^{bc}	-0.02	19,302.339(5)	0.008	19,298.61(2) ^{bc}	-0.03
2	19,314.944(8) ^{bc}	-0.008	19,303.823(6) ^b	-0.001	19,296.409(6) ^b	0.017
3	19,320.881(6) ^{bc}	-0.003	19,306.049(5)	0.002	19,294.924(5) ^b	0.011
4	19,327.559(6) ^b	0.003	19,309.018(5)	0.003	19,294.157(5) ^{bc}	-0.010
5	19,334.979(5) ^b	0.007	19,312.731(5)	0.003	19,294.157(5) ^{bc}	-0.005
6	19,343.131(5) ^b	0.011	19,317.197(5) ^b	0.002	19,294.896(5) ^b	-0.005
7	19,352.026(5) ^b	0.004	19,322.484(5) ^b	0.008	19,296.378(5) ^b	-0.004
8	19,361.662(5) ^b	0.003	19,328.131(5)	0.005	19,298.610(5) ^{bc}	0.011
9	19,372.038(5)	0.005	$19,334.890(5)^{b}$	0.002	19,301.576(5)	0.003
10	19,383.157(5)	0.001	19,342.323(5)	0.005	19,305.287(5)	0.002
11	19,395.008(5)	-0.001	19,350.488(5)	-0.002	19,309.745(5) ^{bc}	0.007
12	19,407.618(5)	-0.006	19,359.384(5) ^b	-0.003	19,314.944(5) ^{bc}	0.001
13	$19,420.971(5)^{b}$	0.008	19,369.040(5)	-0.008	19,320.881(5) ^{bc}	-0.002
14	19,435.052(5)	0.004	19,379.437(5)	0.004	19,327.583(5) ^b	-0.007
15	19,449.880(5)	0.005	19,390.570(5)	0.001	19,335.026(5) ^b	0.001
16	19,465.455(5)	-0.001	19,402.449(5)	0.003	19,343.217(5) ^b	0.002
17	19,481.775(5) ^b	0.002	19,415.076(5)	-0.004	19,352.158(5) ^b	0.005
18	19,498.843(5)	-0.002	19,428.451(5)	-0.002	19,361.853(5) ^b	-0.001
19	19,516.666(5)	0.002	19,442.576(5)	-0.004	19,372.305(5)	0.002
20	19,535.244(5) ^b	0.001	19,457.454(5)	-0.002	19,383.524(5)	0.001
21	19,554.601(5)	0.001	19,473.090(5) ^b	0.001	19,395.522(5)	0.002
22	19,574.768(5) ^b	-0.005	19,489.489(5)	-0.001	19,408.336(5)	0.004
23	19,595.859(5)	-0.005	$19,506.670(5)^{b}$	-0.004	19,422.076(5)	0.003
24	19,618.480(5)	-0.009	19,524.651(5)	-0.005	19,437.366(5)	-0.003
25	19,635.871(5)	0.003	19,543.478(5)	-0.007	19,447.429(5)	0.001
26	19,660.719(6) ^b	-0.004	19,563.324(5) ^b	0.003	19,464.952(5)	-0.001
27	19,684.925(6) ^b	0.007	19,584.862(5)	0.005	19,481.844(5) ^b	0.006
28	19,709.672(7) ^b	0.002	19,596.601(5)	0.001	19,499.277(5)	-0.003
29	19,735.156(5)	-0.003	19,621.900(5)	-0.007	19,517.465(6) ^b	0.007
30	19,761.578(8) ^b	-0.002	19,645.197(5)	-0.008	19,536.606(5)	-0.004
31	19,789.94(1) ^b *	-	$19,668.690(6)^{b}$	0.006	19,557.679(5)*	-
32	19,812.67(1) ^b *	-	19,692.791(5) ^b	0.010	19,573.139(6)*	-
33	19,843.65(2) ^b *	-	19,718.777(6)*	-	19,596.877(9)*	-
34	19,871.389(7)	-0.003	19,742.784(5)	0.001	$19,617.346(8)^{b}$	0.004
35	19,901.477(9)	0.014	19,769.195(5)	0.009	19,640.151(8) ^b	-0.003
36	19,932.86(1)	0.01	19,796.999(6)	-0.001	19,664.342(8)	-0.002
37	19,962.15(1)	-0.02	19,821.850(9) ^b	0.018	$19,686.41(2)^{b}$	-0.01
38	19,994.88(3) ^{bw}	0.02	19,851.273(7)	0.003	19,711.91(2) ^b	0.02
39	a column lists obse		19,880.862(7)	-0.01	19,738.56(3) ^b	0.02

^a The o-c column lists observed minus calculated frequencies. The instrumental resolution was 0.018 cm⁻¹. The estimated absolute calibration uncertainty was 0.004 cm⁻¹. The uncertainties in parentheses indicate 1σ standard deviations and are a combination of fitting and calibration errors. The absolute accuracy of line frequencies is estimated to be $0.006 - 0.01 \text{ cm}^{-1}$ depending on the line intensity and blending.

b Lines marked with b and/or w are blended and/or weak.

^c Lines that do not meet the resolution criterion. The transition frequencies of the thus blended lines in the given contour have been assigned to the strongest line.

* The lines marked with an asterisk were not used in the final fit (see Discussion for details).

Table 4 Transition frequencies (in cm $^{-1}$) of the $C^1\Sigma^+$ – $A^1\Pi(0,2)$ VIS-FT emission band in $^{12}C^{18}O.^{a,b}$

	• `	m cm) or the C 2	,	1 Cilission band		
J''	R(J'')	O-C	Q(J'')	<i>0-C</i>	P(J'')	0-с
1	-	-	24,304.45(3) ^{bw}	-0.02	24,300.74(6) ^{bw}	-0.04
2	24,317.04(3) ^{bw}	-0.01	24,305.94(3) ^b	-0.01	24,298.53(3) ^{bw}	-0.01
3	24,322.94(2) ^w	-0.01	24,308.12(2) ^b	-0.02	24,297.02(4) ^{bw}	-0.02
4	24,329.57(3) ^b	-0.01	24,311.06(2) ^b	-0.02	24,296.26(3) ^b	0.01
5	$24,336.94(2)^{b}$	-0.01	24,314.76(2) ^b	0.02	24,296.22(2) ^b	-0.01
6	$24,345.06(2)^{b}$	0.02	24,319.15(2) ^b	-0.02	24,296.92(2) ^b	-0.01
7	$24,353.86(2)^{b}$	-0.02	24,324.395(8) ^b	-0.004	24,298.34(2) ^b	-0.02
8	$24,363.43(2)^{b}$	-0.02	24,330.000(9) ^b	0.021	24,300.52(2) ^b	-0.01
9	$24,373.75(2)^{b}$	0.01	24,336.68(1) ^b	0.007	24,303.44(2) ^b	0.02
10	24,384.778(7)	0.001	24,344.025(8) ^b	-0.003	24,307.08(1) ^b	0.01
11	24,396.541(7)	-0.007	24,352.121(7) ^b	0.011	24,311.45(1) ^b	-0.01
12	24,409.048(8)	-0.006	24,360.927(7) ^b	0.001	24,316.561(9) ^b	-0.004
13	$24,422.29(2)^{b}$	0.01	24,370.459(7) ^b	-0.019	24,322.413(9) ^b	-0.009
14	24,436.254(7)	-0.004	$24,380.764(7)^{b}$	0.009	24,329.008(9) ^b	-0.011
15	24,450.962(8)	-0.009	24,391.761(7) ^b	-0.017	$24,336.35(1)^{b}$	0.005
16	24,466.408(8)	-0.011	24,403.542(8) ^b	0.001	24,344.43(1) ^b	0.003
17	24,482.600(8)	-0.001	$24,416.034(7)^{b}$	-0.009	24,353.23(1) ^b	-0.02
18	24,499.525(9)	-0.003	24,429.288(8) ^b	0.009	24,362.80(2) ^b	-0.02
19	$24,517.18(2)^{b}$	-0.03	24,443.274(9) ^b	0.011	$24,373.14(2)^{b}$	0.01
20	$24,535.62(2)^{b}$	-0.04	24,458.000(9) ^b	-0.001	24,384.20(2) ^b	-0.02
21	24,554.84(3) ^b	-0.01	$24,473.49(1)^{b}$	0.01	24,396.09(2) ^b	0.03
22	24,574.81(3) ^{bw}	-0.04	24,489.74(1) ^b	0.01	$24,408.71(2)^{b}$	-0.03
23	24,595.76(3) ^b	-0.01	24,506.75(2) ^b	0.01	$24,422.31(2)^{b}$	-0.01
24	24,618.23(4) ^{bw}	0.02	24,524.54(2) ^b	-0.02	24,437.44(2) ^b	0.01
25	24,635.42(4) ^{bw}	-0.01	24,543.20(2) ^b	-0.02	24,447.33(2) ^b	0.01
26	24,660.07(5) ^{bw}	-0.03	24,562.87(2) ^{bc}	-0.01	24,464.68(2) ^b	-0.01
27	24,684.11(6) ^{bw}	-0.01	24,584.22(2) ^b	-0.01	$24,481.40(2)^{b}$	0.01
28	$24,708.67(2)^{\text{w}}$	0.01	24,595.81(4) ^{bw}	0.02	24,498.66(2) ^b	0.01
29	24,733.96(5) ^{bw}	-0.02	24,620.88(5) ^{bw}	-0.03	24,516.66(3) ^b	0.01
30	, , , ,		24,644.02(3) ^b	0.01	, , ,	
31			24,667.32(3) ^{bw}	0.01		
32			24,691.24(4) ^{bw} *	-		
33			24,717.03(6) ^{bw} *	_		
34			24,740.85(3) ^w	0.01		
35			24,767.03(5) ^{bw}	0.02		
a The	a aalumn lista	alagariad rainus as	laulated frequenci		atal ragalution is	0.010 am ⁻¹ T

^a The o-c column lists observed minus calculated frequencies. The instrumental resolution is 0.018 cm⁻¹. The estimated absolute calibration uncertainty is $0.004~\rm cm^{-1}$. Uncertainties in parentheses indicate 1σ standard deviations and are a combination of fitting and calibration errors. The absolute accuracy of the frequencies is estimated to be $0.01-0.02~\rm cm^{-1}$, depending on the line intensity and blending.

b Lines marked with b and/or w are blended and/or weak.

^c Lines that do not meet the resolution criterion. The transition frequencies of the thus blended lines in the given contour have been assigned to the strongest line.

The lines marked with an asterisk were not used in the final fit (see Discussion for details).

Table 5 Transition frequencies of the interaction-induced (in cm⁻¹) observed in the $B^1\Sigma^+ - A^1\Pi(0, 2)$ and $C^1\Sigma^+ - A^1\Pi(0, 2)$ VIS-FT emission bands in ¹²C¹⁸O. ^{a,b,c}

$J^{\prime\prime}$	${}^{s}R_{11ee}$	0-с	$^qQ_{12ef}$	0-С	$^qQ_{11e\!f}$	0-с	$^qP_{11ee}$	0-с	$^rQ_{11ef}$	0-С
					$B^{1}\Sigma^{+}-e^{3}\Sigma^{-}$, 4)				
24 25	19,602.51(2) ^b 19,648.632(8) ^b	-0.02 0.022					19,421.392(9) 19,460.17(2) ^b	-0.014		
26	19,048.032(8)	0.022	19,526.76(3) ^{bw}	-0.01			19,400.17(2)	0.01		
27			19,563.44(2) ^b	0.01						
28			19,612.074(5)*	-	plp+ 3. (0					
					$\mathbf{B}^{1}\boldsymbol{\Sigma}^{+}-\mathbf{d}^{3}\boldsymbol{\Delta}\;(0$, 7)				
33	19,840.46(2) ^b	-0.01							19,715.48(2) ^b	0.01
36										
37										
					$\mathbf{B}^{1}\boldsymbol{\Sigma}^{+}-\mathbf{I}^{1}\boldsymbol{\Sigma}^{-}(0$, 3)				
7					19,319.73(2)	0.01				
8					19,331.281(9)	0.003				
					$C^1\Sigma^+ - e^3\Sigma^- (0$, 4)				
27			24,562.87(4) ^{bw} *	-						
					$C^{1}\Sigma^{+}-I^{1}\Sigma^{-}$, 3)				
8			lioto - olo		24,333.13(3) ^w	0.01				

^a The *o-c* column lists observed minus calculated frequencies. The uncertainties in parentheses indicate 1σ standard deviations and are a combination of fitting and calibration errors.

b Lines marked with b and/or w are blended and/or weak.

The superscripts p, q, r and s denote change in the total angular momentum excluding spin.

The lines marked with an asterisk were not used in the final fit (see Discussion for details).

Table 6 Couplings considered in the deperturbation analysis of the $A^1\Pi(v=2)$ level in $^{12}C^{18}O$.

Nº	Analysed interactions	Nature	Took part in the final	Status ^a	Notes ^b
1	$A^{1}\Pi(v=2) \sim I^{1}\Sigma^{-}(v=2)$	Rotation-electronic	fit No	_	Negligible.
1	$A \Pi(v=2) \sim 12 (v=2)$	(<i>L</i> -uncoupling)	NO	-	Negligible.
2	$\sim I^1 \Sigma^- (v=3)$	(E uncoupring)	Yes	Floated	-
3	$\sim I^1 \Sigma^- (v = 4)$	"	Yes	Floated	
4	$\sim I^1 \Sigma^- (v = 5)$	"	No	-	Negligible.
5	$\sim e^3 \Sigma^{-} (v=2)$	Spin-orbit	No	-	Negligible.
6	$\sim e^3 \Sigma^- (v=3)$	"	Yes	Fixed	Noticeable. Statistically unjustified.
7	$\sim e^3 \Sigma^- (v = 4)$	"	Yes	Floated	
8	$\sim e^3 \Sigma^- (v = 5)$	"	No	-	Negligible.
9	$\sim d_2^3 \Delta(v=6)$	"	No	-	Negligible.
10	$\sim d^3 \Delta(v=7)$	"	Yes	Floated	
11	$\sim d^3 \Delta(v=8)$	"	Yes	Fixed	Noticeable. Statistically unjustified.
12	$\sim d^3 \Delta(v=9)$, "	No	-	Negligible.
13	$\sim a'^3 \Sigma^+ (v = 11)$,	No	-	Negligible.
14	$\sim a'^3 \Sigma^+ (v = 12)$,	Yes	Floated	-
15	$\sim a'^3 \Sigma^+ (v = 13)$	s) "	Yes	Fixed	Noticeable. Statistically unjustified.
16	$\sim a'^3 \Sigma^+ (v = 14)$) "	No	-	Negligible.
17	$\sim D^1 \Delta(v=2)$	Rotation-electronic (<i>L</i> -uncoupling)	No		Negligible.
18	$\sim D^1 \Delta(v=3)$	(L-uncouping)	Yes	Floated	-
19	$\sim D^1 \Delta (v = 4)$	"	No	10000	Negligible.
20	$d^3\Delta(v=7) \sim e^3\Sigma^-(v=4)$	Spin-spin	No		Statistically unjustified. If floated, it correlates
	, , , ,	1 1			with $<$ A(2) LS e(4)>. No theoretical value
					available.
21	$\sim a'^3 \Sigma^+ (v = 12)$	2) "	No	-	Statistically unjustified. No theoretical value
					available.
22	$e^{3}\Sigma^{-}(v=4) \sim a'^{3}\Sigma^{+}(v=12)$	Spin-orbit	No	-	Statistically unjustified. If floated, it correlates
					with $<$ A(2) LS e(4)> and $<$ A(2) LS a'(12)>. No
22	3m/ 10) rlp=/ 0)	,,	3.7		theoretical value available.
23	$a^{3}\Pi(v = 13) \sim I^{1}\Sigma^{-}(v = 3)$ $\sim e^{3}\Sigma^{-}(v = 4)$		No	- -	Negligible indirect impact on A(2).
24	$\sim e^{s} \Sigma (v=4)$	Spin-orbit /	Yes	Fixed	Noticeable. If floated, it correlates with B and λ
		spin-electronic			constants of e(4).
25	$\sim e^3 \Sigma^- (v = 4)$	L-uncoupling	Yes	Fixed	Noticeable. Statistically unjustified.
26	$\sim \frac{62}{5}(v-4)$ $\sim \frac{d^3\Delta(v=7)}{5}$	Spin-orbit /	Yes	Fixed	Noticeable. If floated, it correlates with <i>B</i>
20	- u Δ(ν γ)	spin-electronic	1 03	1 IXCU	constant of $d(7)$.
27	$\sim d^3\Delta(v=7)$	L-uncoupling	Yes	Fixed	Noticeable. Statistically unjustified.
28	$\sim a^{13}\Sigma^{+}(\nu = 12)$	Spin-orbit /	Yes	Fixed	Noticeable. Statistically unjustified.
_0	a 2 () – 12	spin-electronic	- •0		2
29	$\sim a^{3}\Sigma^{+}(v=12)$	L-uncoupling	Yes	Fixed	Noticeable. Statistically unjustified.
30	$\sim D^{1}\Delta(v=3)$	Spin-orbit	Yes	Fixed	Noticeable. Statistically unjustified.
	(, 3)	~F-11 01011	- 40		······································

^a Whether parameters are floated during optimisation or fixed to their theoretical values.

^b Whether there is a noticeable influence of the floated parameter on the frequencies of observed lines. This was checked by comparing frequencies computed with parameters floated, fixed to calculated values, or set to zero.

-21- Table 7 Deperturbed molecular parameters of the $A^1\Pi(\nu=2)$ level and its perturbers in $^{12}C^{18}O.^{a,b}$

Constant	$A^{1}\Pi(v=2)$	$A^1\Pi(v=2)$	$A^{1}\Pi(v=2)$	$e^{3}\Sigma^{-}(v=3)$	$e^3\Sigma^-(v=4)$	$e^3\Sigma^-(v=4)$	$e^3\Sigma^-(v=4)$
		Ref. [17]	Ref. [16]		` _	Ref. [17]	Ref. [16]
T_{ν}	67,615.36028(66)	67,616.7522 (81)	67,616.78(1)	66,870.96 ^t	67,883.7853(23)	67,884.44	67,884.44
B	1.48521967(84)	1.485101(54)	1.48522(6)	1.16 ^g	1.1491305(61)	1.14897	1.14897
$q \times 10^{5}$	-1.31 ^e						
$D \times 10^6$	6.7556(34)	6.65	6.9	6.10^{g}	6.07 ^g	6.14	6.3
$H \times 10^{12}$	-48.2(18)			-1.73 ^h	-1.73 ^h		
λ				0.57^{s}	0.9541(92)	0.69	0.70
η					-13.0234(36)	-12.68^{i}	$-12.6(5)^{i}$
$\eta_{theoret}^{\text{c}}$				12.38	-12.84		
$\eta_{theoret}$ $\delta \eta^{ ext{d}}$				4	1.4		
Constant	$d^3\Delta(v=7)$	$d^3\Delta(v=7)$	$d^3\Delta(v=8)$		$a'^3\Sigma^+(v=12)$	$a'^3\Sigma^+(v=12)$	$a'^3\Sigma^+(v=13)$
Constant		Ref. [16]				Ref. [16]	` '
T_{ν}	68,097.610(75)	68,102.72	69,090.91 ^f		68,249.455(23)	68,249.47	69,203.30 ^f
В	1.129309(88)	1.12927	1.11 ^g		1.08 ^g	1.08361	1.07 ^g
4	-16.61 ^g		-16.77 ^g	_ / \			
$D \times 10^{6}$	5.83 ^g	5.7	5.82 ^g		5.67 ^g	5.7	5.66 ^g
$H \times 10^{12}$	-0.69^{h}		-0.69 ^h	/1	-0.35 ^h		-0.35^{h}
$A_D \times 10^5$	-9.62^{j}		-9.62^{j}				
λ	1.07^{s}	1.20	1.17 ^s		-1.11 ^s	-1.10	-1.10^{s}
$\gamma \times 10^2$	-0.81 ^j	-0.83	0.88^{j}		-0.50^{j}		-0.48^{j}
η	-10.076(27)	-10.7^{i}			-5.688(29)	5.5 ⁱ	
$\eta_{theoret}^{c}$	-10.18		13.97		-5.73		4.54
$\eta_{theoret}$ $\delta \eta^{ ext{d}}$	1.6				0.04		

Table 7 - continued.

Constant	$a^3\Pi(\nu=13)$	$I^1\Sigma^-(v=3)$	$I^{1}\Sigma^{-}(v=3)$ Ref. [17]	$I^{1}\Sigma^{-}(v=3)$ Ref. [16]	$I^{1}\Sigma^{-}(\nu=4)$	$D^1\Delta(v=3)$	$D^{1}\Delta(v = 3)$ Ref. [16]
T_{v}	68,067.55 ^k	67,636.2405(60)	67,635.91(68)	67,636.0(6)	68,622.51°	68,431.16 ^p	68,431.42
B	1.36 ^g	1.15 ^g	1.15147	1.15147	1.13 ^g	1.14 ^r	1.13967
0	0.63^{1}						
$p \times 10^3$	2.73 ^m						
$q \times 10^5$	3.01^{1}						
A	37.48 ^g						
$D \times 10^{6}$	6.29^{g}	6.26 ^h	6.24	6.3	6.28 ^h	6.33 ^r	6.3
$H \times 10^{12}$	m	2.59 ^h			2.59 ^h	-2.59 ^h	
$A_D \times 10^5$	-20 ^m						
$\lambda \times 10^2$	-0.75 ^t						
$\gamma \times 10^2$ $\xi \times 10^2$	0.32 ^j	5 (22(20)	£ 20(6£)İ	-5.7(4) ⁱ	0.21(20)	2.50(25)	-4 ⁱ
ζ × 10		-5.633(39)	$-5.39(65)^{i}$	-3.7(4)	8.31(28)	3.50(25) 2.90	-4
$(\xi_{theoret} \times 10^2)^{c}$ $\delta \xi^{d}$		-5.30 6.5			6.75 21.6	20.2	
$\eta (\sim I, v = 3)$	-11.47 ^u	0.3			21.0	20.2	
$\eta(\sim 1, v = 3)$ $\eta(\sim e, v = 4)$	24.07 ^w						
$\xi(\sim e, v = 4)$	0.06 ^w						
$\eta(\sim d, v = 7)$	16.45 ^w						
$\xi(\sim d, v = 7)$	-0.04 ^w						
$\eta(\sim a', v = 12)$	4.52 ^w						
$\xi(\sim a', v = 12)$	-0.01 ^w						
$\eta (\sim D, v = 3)$	-22.78 ^u						

 $[\]overline{}^a$ All quantities have units of cm $^{-1}$ apart from relative percentage errors $\delta \eta$ and $\delta \xi$. Some T and B constants are fixed to or initialised from literature data (possibly scaled from other isotopologues) given in terms of the \hat{R} rotation operator, while most values in this are fitted to

way of obtaining the vibrational overlap integrals $(v_A|v_{a',e,d})$ and rotational operator integrals $(v_A|\widehat{B(R)}|v_{I,D})$ is highlighted in Refs. [13,14].

^d Relative errors expressed as difference between theoretical and fitted values as a percentage: $\delta \eta = \frac{(\eta_{theoret} - \eta)}{\eta_{theoret}} \times 100\%$; $\delta \xi = \frac{(\xi_{theoret} - \xi)}{\xi_{theoret}} \times 100\%$

Government of Calculated on the basis of Refs. [11,45] and isotopic scaling.

Government of Calculated in this work on the basis of Refs. [6,22] and isotopic scaling.

Calculated from Ref. [6] based on mass-scaling.

Calculated in this work on the basis of Ref. [8] by isotopic scaling.

The η and ζ parameters were calculated from α and β constants from Ref. [17] or Ref. [16] based on Eqs. (1) - (3) in Ref. [19].

- 23 -

- ^j Taken from Ref. [6] (in MHz), then converted into cm⁻¹ and isotopically scaled.
- ¹Taken from Ref. [6] (in MHz), then converted into cm² and isotopically scaled. ¹Calculated on the basis of Refs. [6,22,46] and isotopically scaled where necessary. ¹Calculated in this work on the basis of Ref. [47] ($o = C^{\circ}$ or $q = 2 \times B_{\theta_{+}}$) by isotopic scaling. ¹Calculated in this work on the basis of Ref. [48] ($p = 2 \times p_{+}$) by isotopic scaling. ²Calculated in this work on the basis of Refs. [6,49] by isotopic scaling. ³Colculated on the basis of Ref. [31] by isotopic scaling. ⁴Calculated in this work on the basis of Ref. [31] by isotopic scaling.

- ⁸ Calculated in this work on the basis of Ref. [6] (diagonal spin-spin constant $\lambda = -1.5 \times C$ in MHz), converted into cm⁻¹ and isotopically scaled. ¹ Calculated in this work on the basis of Ref. [48] (diagonal spin-spin constant $\lambda = 1.5 \times \epsilon$ in MHz), converted into cm⁻¹ and isotopically scaled. ^u Theoretical spin-orbit interaction parameters were calculated on the basis of the electronic a_{a-1} parameter given by Field et al. [7] or a_{a-D} parameter from Garetz et. al [50] as well as $\alpha_{a-1}(a_{a-1})$ or $\alpha_{a-D}(a_{a-D})$ perturbation parameter dependences given by Field et. al [1,7]. The $\eta_{a-1}(a_{a-D})$ and $\eta_{a-D}(a_{a-D})$ relationships follow from symmetrized matrix elements of the $a^3\Pi \sim 1^1\Sigma^-$ and $a^3\Pi \sim 0^1\Delta$ interactions. A way of obtaining the vibrational overlap integrals $\langle v_a | v_{I,D} \rangle$ has the same methodology as in Refs. [13,14,28].
- Theoretical spin-orbit (together with spin-electronic) and L-uncoupling interaction parameters were calculated on the basis of electronic $a_{a \sim e,d,a'}$ and $b_{a \sim e,d,a'}$ parameters given by Field et al. [7] as well as $\alpha_{a \sim e,d,a'}(a_{a \sim e,d,a'})$ and $\beta_{a \sim e,d,a}(b_{a \sim e,d,a'})$ dependencies given by Field et. al [1,7]. The $\eta_{a\sim e,d,a'}(\alpha_{a\sim e,d,a'})$ and $\xi_{a\sim e,d,a'}(\beta_{a\sim e,d,a'})$ relationships follow from e/f-symmetrized matrix elements of the $a^3\Pi\sim e^3\Sigma^-$, $d^3\Delta$, $a'^3\Sigma^+$ interactions. A way of obtaining the vibrational overlap integrals $\langle v_a | v_{e,d,a'} \rangle$ and rotational operator integrals $\langle v_a | \overline{B(R)} | v_{e,d,a'} \rangle$ involves the same methodology as in Refs. [13,14,28]. The spin-orbit and spin-electronic interactions have the same Ω dependence, which makes it impossible to determine them independently; thus, the $\eta_{a-e,d,d'}$ perturbation parameters represent a linear combinations of both of these interactions.

Table 8 · 120180 a.b.c.d

\overline{J}	Term va	alues (in cm	$(v = 1)^{-1}$ of the A ¹ $\Pi(v = 1)$	2) level and	l its perturbers in 1	$\frac{{}^{2}\mathrm{C}^{18}\mathrm{O}^{a,b,c,a}}{\mathrm{e}^{3}\Sigma^{-}(\mathrm{e}^{3}\mathrm{e}^$		$I^{I}\Sigma^{-}(v=3)$		
					•	¹ Π	, , , , , , , , , , , , , , , , , , ,	1П		¹ Π
	F_{1e} (cm ⁻¹)	$^{1}\Pi\left(\right)$	F_{1f} (cm ⁻¹)	$^{1}\Pi \left(\right)$	F_{1e} (cm ⁻¹)	(%)	F_{2f} (cm ⁻¹)	(%)	F_{1f} (cm ⁻¹)	(%)
1	67618.07(2)	99.89	67618.057(9)	99.89						
2	67623.994(7)	99.89	67623.993(8)	99.88						
3	67632.899(6)	99.89	67632.898(7)	99.87						
4	67644.783(6)	99.89	67644.770(7)	99.83						
5	67659.624(5)	99.89	67659.605(7)	99.74						
6	67677.437(5)	99.88	67677.401(7)	99.39						
7	67698.217(5)	99.88	67698.081(6)	95.11					67,700.85(2)	4.78
8	67721.956(5)	99.88	67722.104(6)	95.15					67,718.96(2)	4.73
9	67748.661(5)	99.87	67748.727(7)	99.18						
10	67778.330(5)	99.86	67778.379(6)	99.59						
11	67810.960(5)	99.85	67810.996(6)	99.70						
12	67846.547(5)	99.84	67846.584(6)	99.75						
13	67885.087(5)	99.83	67885.130(6)	99.77						
14	67926.583(5)	99.81	67926.614(6)	99.77						
15	67971.026(5)	99.79	67971.066(6)	99.76						
16	68018.417(5)	99.76	68018.455(6)	99.75						
17	68068.746(5)	99.72	68068.798(6)	99.73						
18	68122.019(5)	99.67	68122.065(6)	99.70						
19	68178.215(5)	99.58	68178.280(6)	99.66						
20	68237.340(5)	99.44	68237.427(7)	99.60						
21	68299.359(5)	99.19	68299.494(7)	99.51						
22	68364.253(5)	98.64	68364.473(7)	99.37						
23	68431.889(5)	96.97	68432.350(7)	99.14						
24	68501.656(5)	87.07	68503.098(7)	98.73	68,517.63(2)	7.84				
25	68580.320(5)	77.44	68576.660(7)	97.86	68,567.57(2)	9.13	68,629.57(4)	2.07		
26	68655.186(6)	96.07	68652.868(8)	95.49	68,626.48(4)	0.87	68,689.43(4)	4.43		
27	68734.347(6)	98.22	68731.045(7)	85.50			68,752.46(2)	14.41		
28	68816.627(6)	98.56	68822.669(8)	61.17			68,807.20(2)	38.73		
29	68901.810(6)	98.11	68904.397(8)	91.64			68,876.98(4)	8.24		
30	68989.693(7)	95.86	68991.771(8)	97.02	. (//)					
31	69079.289(7)	78.25	69082.583(9)	98.41						
32 33	69178.135(8)	86.35	69176.432(9)	98.68						
33 34	69272.35(1)	51.76	69272.025(9)	60.76 98.73						
35	69373.461(8) 69475.833(9)	98.05 98.13	69373.21(1) 69475.66(1)	98.73 98.33						
36	69580.51(1)	89.88	69580.30(2)	89.68						
37	69690.89(2)	94.64	69691.53(2)	88.78	•					
38	69801.46(2)	97.80	69801.77(2)	98.12						
39	69914.48(2)	89.28	69915.46(2)	97.01						
40	70036.63(3)	60.79	70036.31(4)	58.42						
41	70153.65(3)	97.65	70153.30(4)	97.51						
42	70275.96(3)	99.23	70274.74(4)	82.77						
43	70401.33(3)	99.59	70401.43(4)	98.96						
44	70529.57(3)	99.73	70529.58(4)	99.60						
45	70660.67(3)	99.80	70660.63(4)	99.72						
46	70794.55(3)	99.81	70794.50(4)	99.75						
47	70931.24(3)	99.72								
48	71070.56(3)	91.02								
49	71213.14(4)	99.62								
50	71358.12(5)	99.86								
		$a'^3\Sigma^+$ (v =12)		-	$d^3\Delta(v =$	= 7)			
	F_{2e} (cm ⁻¹)		F_{3f} (cm ⁻¹)		F_{1e} (cm ⁻¹)	,	F_{1f} (cm ⁻¹)			-
33					69,275.53(4)	23.20	69,275.32(3)	19.12		
			70.200.000.00	0.04	07,270.00(1)	25.20	0,2,0,00			
42			70,280.988(25)	9.04						
45	70,467.462(34)	0.03	ra givan in ralation	to the V(- 0. I - 0) love1					

^a All values are given in relation to the X(v = 0, J = 0) level. ^b Computed from $^{12}C^{18}O$ A – X(2, 0), B – A(0, 2) and C – A(0, 2) transition energies and $^{12}C^{18}O$ B(0), C(0) terms given by Hakalla et al. [15] using the X(v = 0) term values calculated in this work on the basis of the individual molecular constants published by Coxon et al. [22].

^c "In ()" denotes percentage character of the A¹ $\Pi(v = 2)$ level.

d The values in parentheses indicate random fitting uncertainties.

FIGURES

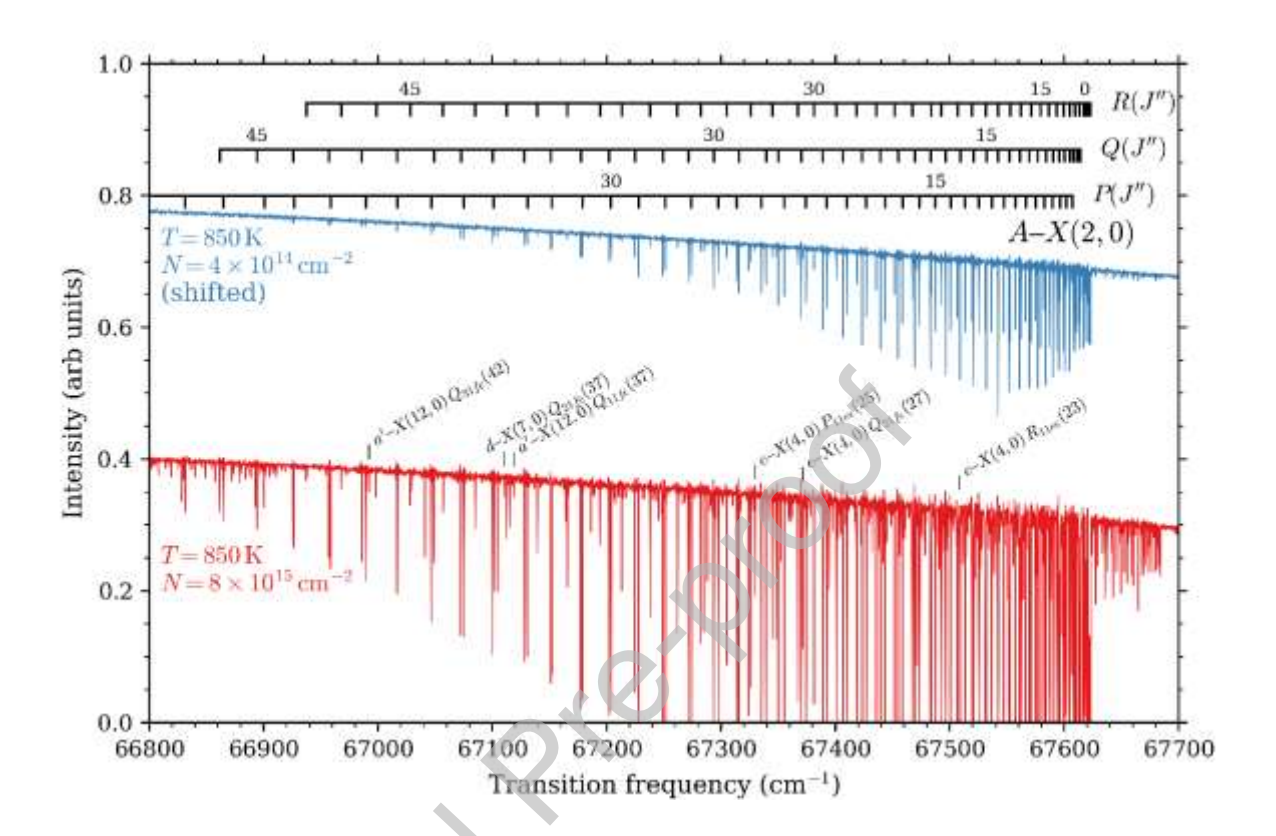


Fig. 1. Two photoabsorption spectra of $^{12}C^{18}O$ $A^{1}\Pi \leftarrow X^{1}\Sigma^{+}(2,0)$ recorded with different column densities. Assigned lines are labelled and the remainder are due to $^{12}C^{16}O$ absorption or $^{12}C^{18}O$ transitions not relevant to this study.

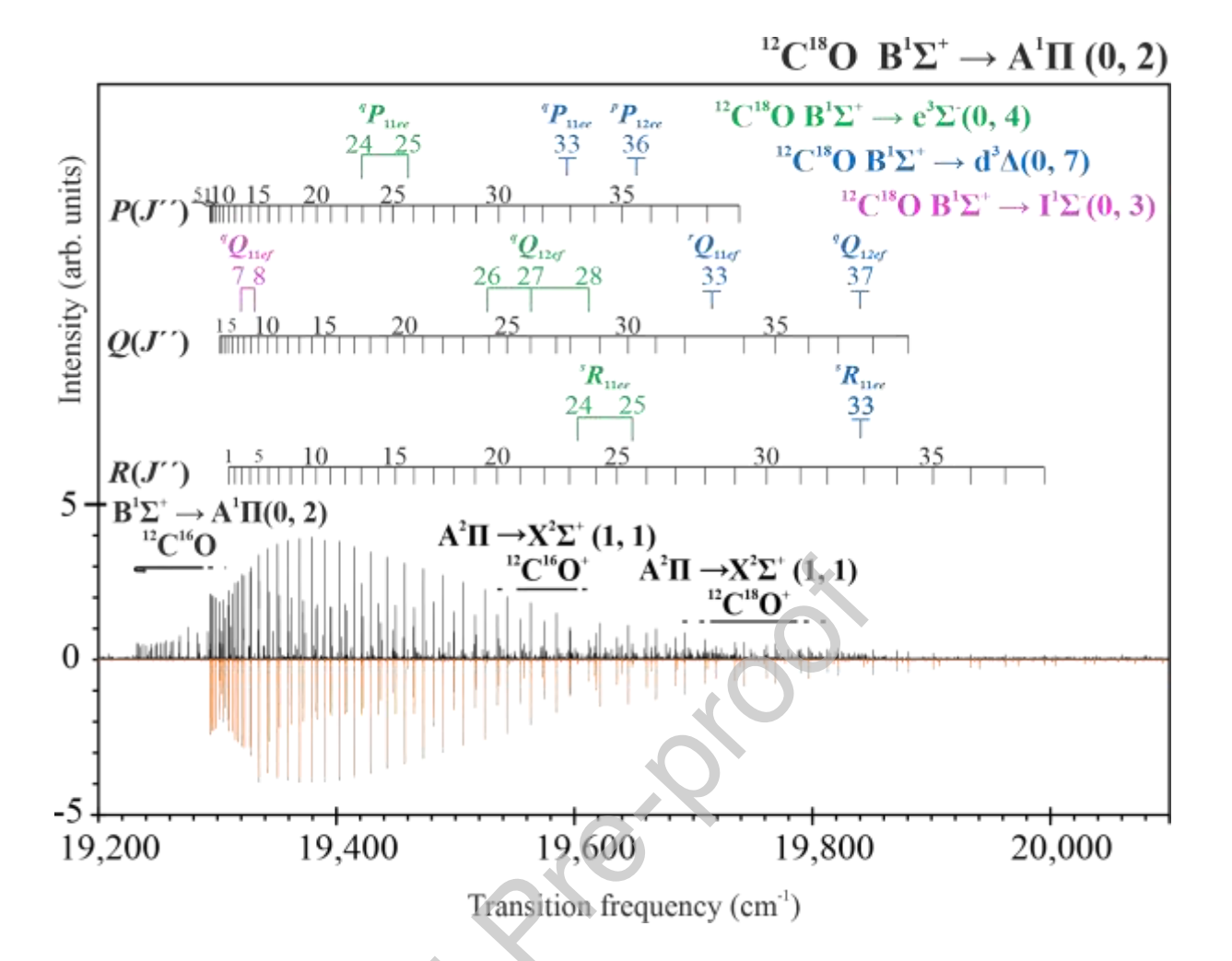


Fig. 2. High-resolution photoemission spectrum of the $^{12}C^{18}O$ B $^{1}\Sigma^{+}$ – A $^{1}\Pi(0, 2)$ band as well as the $^{12}C^{18}O$ B $^{1}\Sigma^{+}$ – e $^{3}\Sigma^{-}(0, 4)$, B $^{1}\Sigma^{+}$ – d $^{3}\Delta$ (0, 7), B $^{1}\Sigma^{+}$ – I $^{1}\Sigma^{-}(0, 3)$ extra-lines, recorded by the FTS technique in the visible region. The upper trace presents an experimental spectrum of the $^{12}C^{18}O$ B $^{1}\Sigma^{+}$ – A $^{1}\Pi(0, 2)$ band with contamination from other isotopologues of carbon monoxide appearing in the spectrum, whereas the lower trace is a simulation after deperturbation of the $^{12}C^{18}O$ B $^{1}\Sigma^{+}$ – A $^{1}\Pi(0, 2)$ band together with the $^{12}C^{18}O$ B $^{1}\Sigma^{+}$ – e $^{3}\Sigma^{-}(0, 4)$, B $^{1}\Sigma^{+}$ – d $^{3}\Delta$ (0, 7), B $^{1}\Sigma^{+}$ – I $^{1}\Sigma^{-}(0, 3)$ extra-lines. The simulation was performed using the PGOPHER software [25,26].

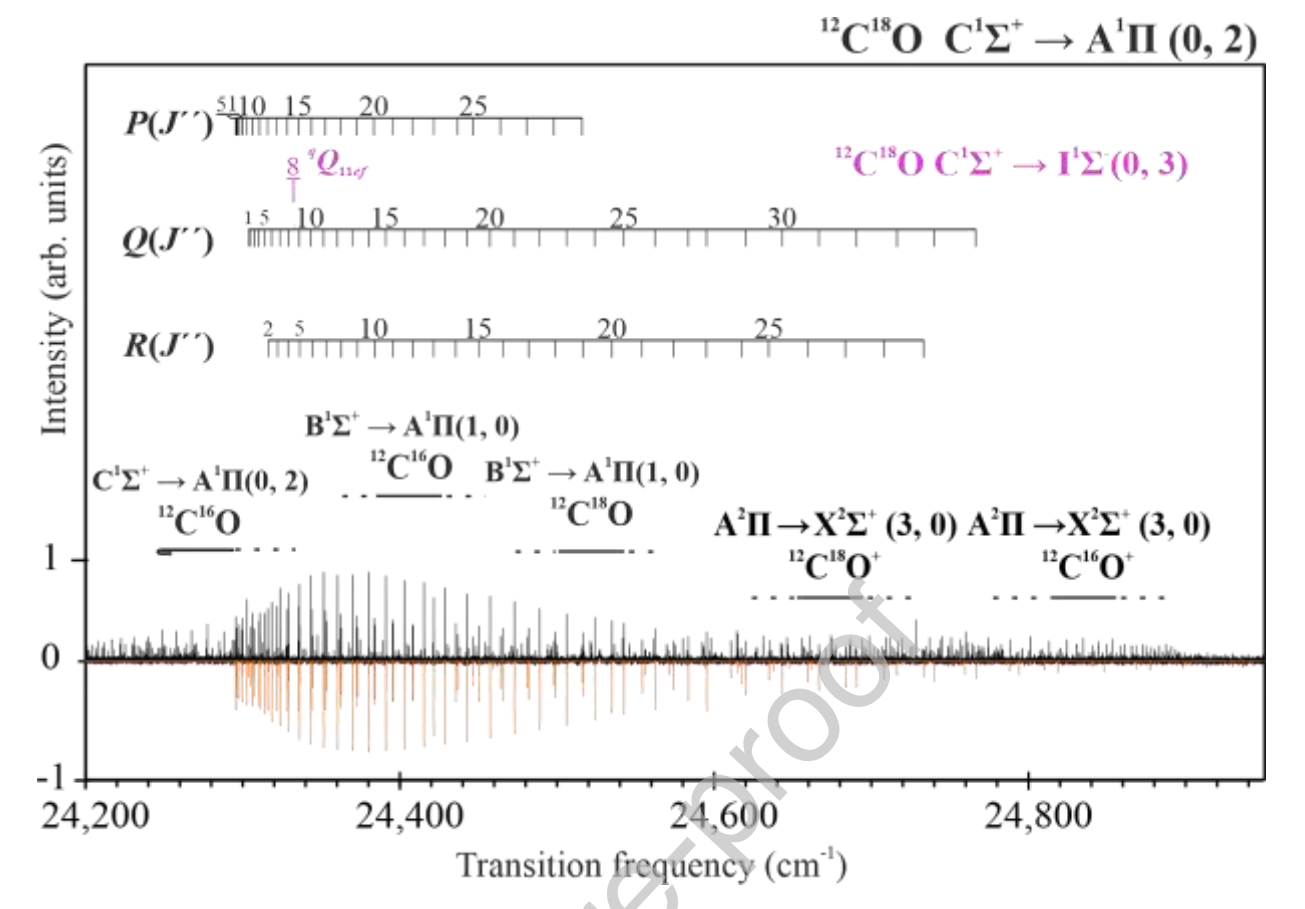


Fig. 3. High-resolution photoemission spectrum of the $^{12}C^{18}O$ $C^1\Sigma^+ - A^1\Pi(0, 2)$ band as well as the $^{12}C^{18}O$ $C^1\Sigma^+ - I^1\Sigma^-(0, 3)$ extra-lines, recorded by the FTS technique in the visible region. The upper trace presents an experimental spectrum of the $^{12}C^{18}O$ $C^1\Sigma^+ - A^1\Pi(0, 2)$ band with contamination from other isotopologues of carbon monoxide appearing in this spectrum, whereas the lower trace is a simulation after deperturbation of the $^{12}C^{18}O$ $C^1\Sigma^+ - A^1\Pi(0, 2)$ band together with the $^{12}C^{18}O$ $C^1\Sigma^+ - I^1\Sigma^-(0, 3)$ extra-lines. The simulation was performed using the PGOPHER software [25,26].

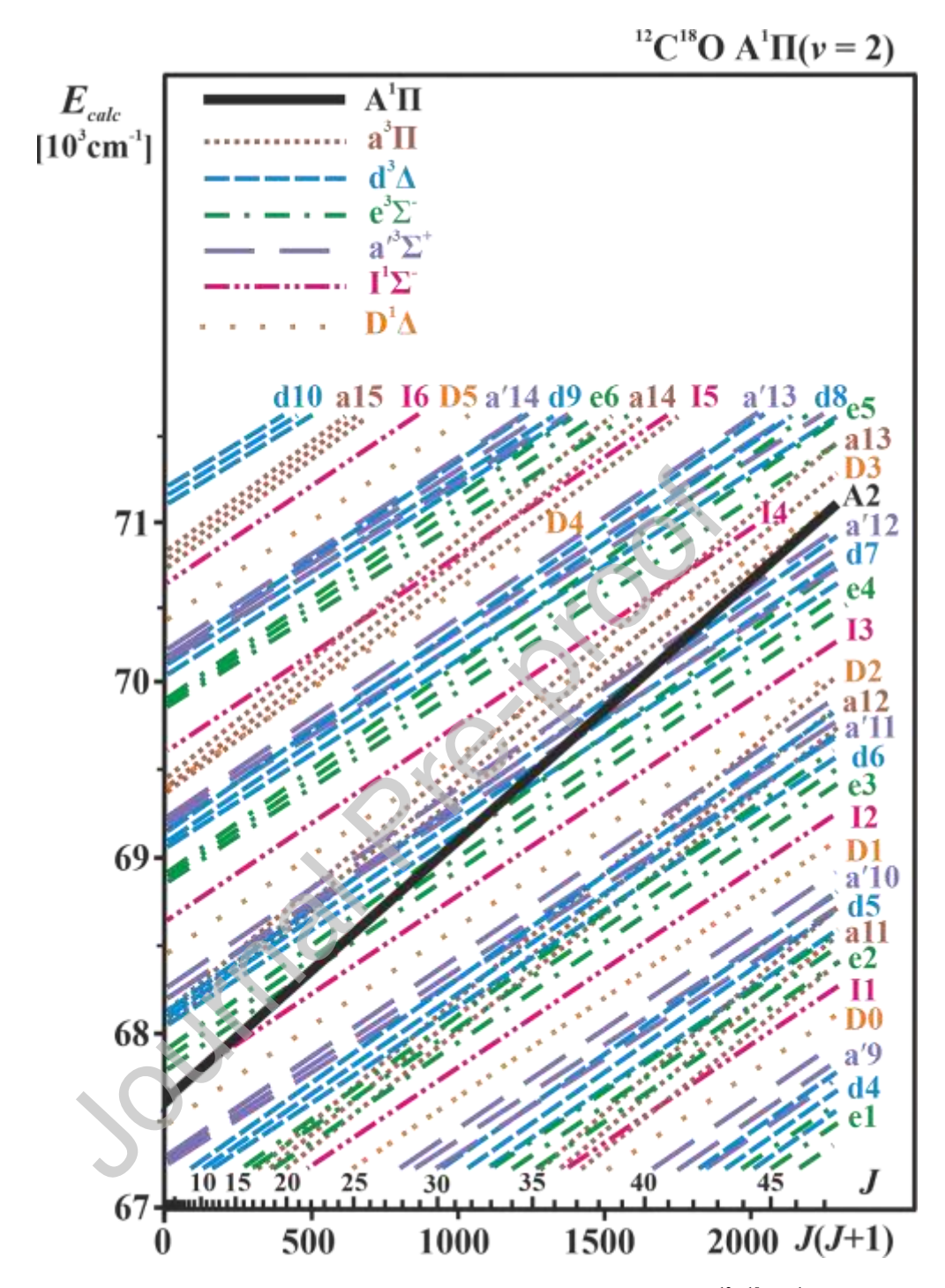


Fig. 4. Ro-vibronic term series in the energy neighbourhood of the $^{12}C^{18}O$ A $^{1}\Pi(\nu = 2)$ level (67,000 - 71,000 cm $^{-1}$). Labels denote the electronic state and the vibrational quantum number.

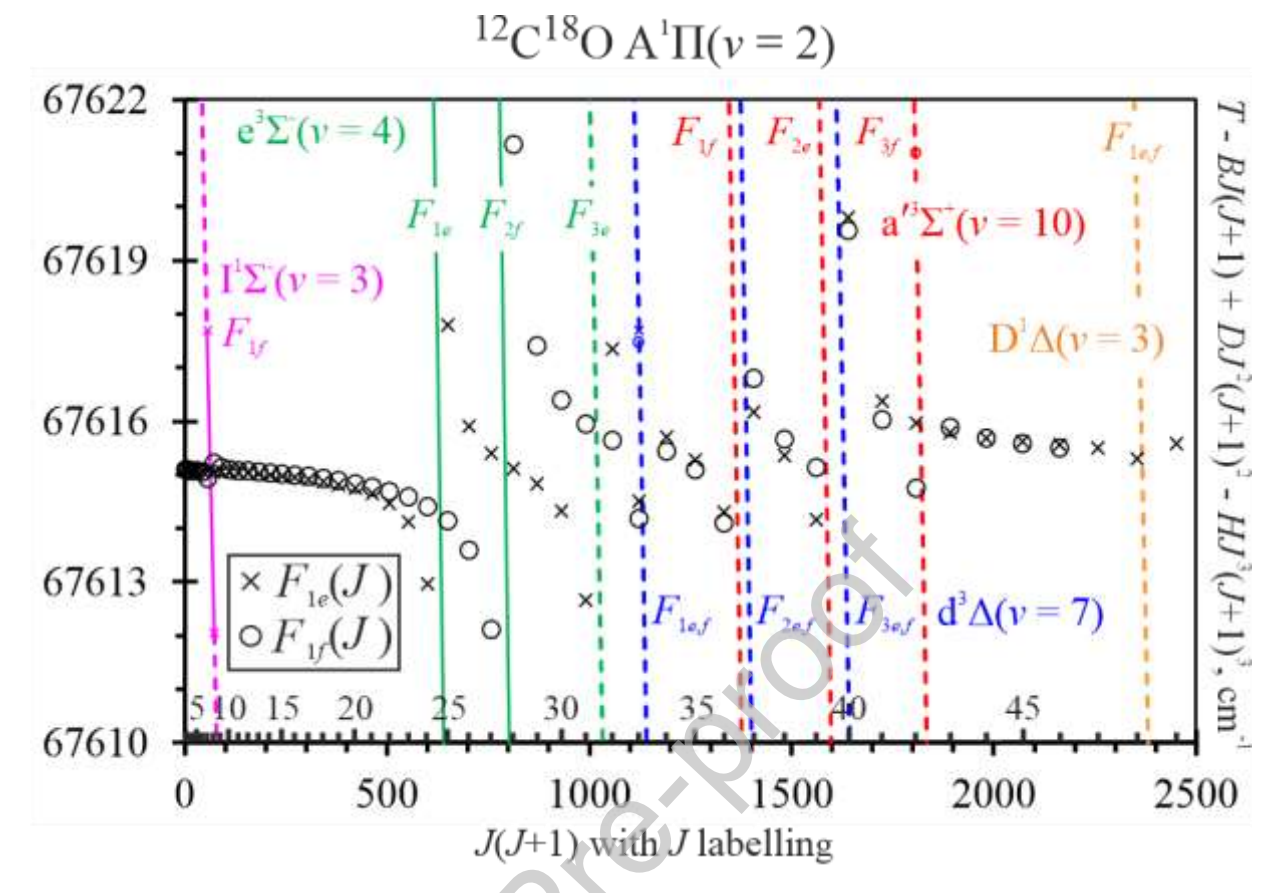


Fig. 5. The experimental reduced term values (in cm⁻¹) of the $^{12}C^{18}O$ A¹ $\Pi(v=2)$ level and its perturbers. The energies are calculated as $T(J) - BJ(J+1) + DJ^2(J+1)^2 - HJ^3(J+1)^3$ for B = 1.48521967 cm⁻¹, $D = 6.7556 \times 10^{-6}$ cm⁻¹ and $H = -4.82 \times 10^{-11}$ cm⁻¹.

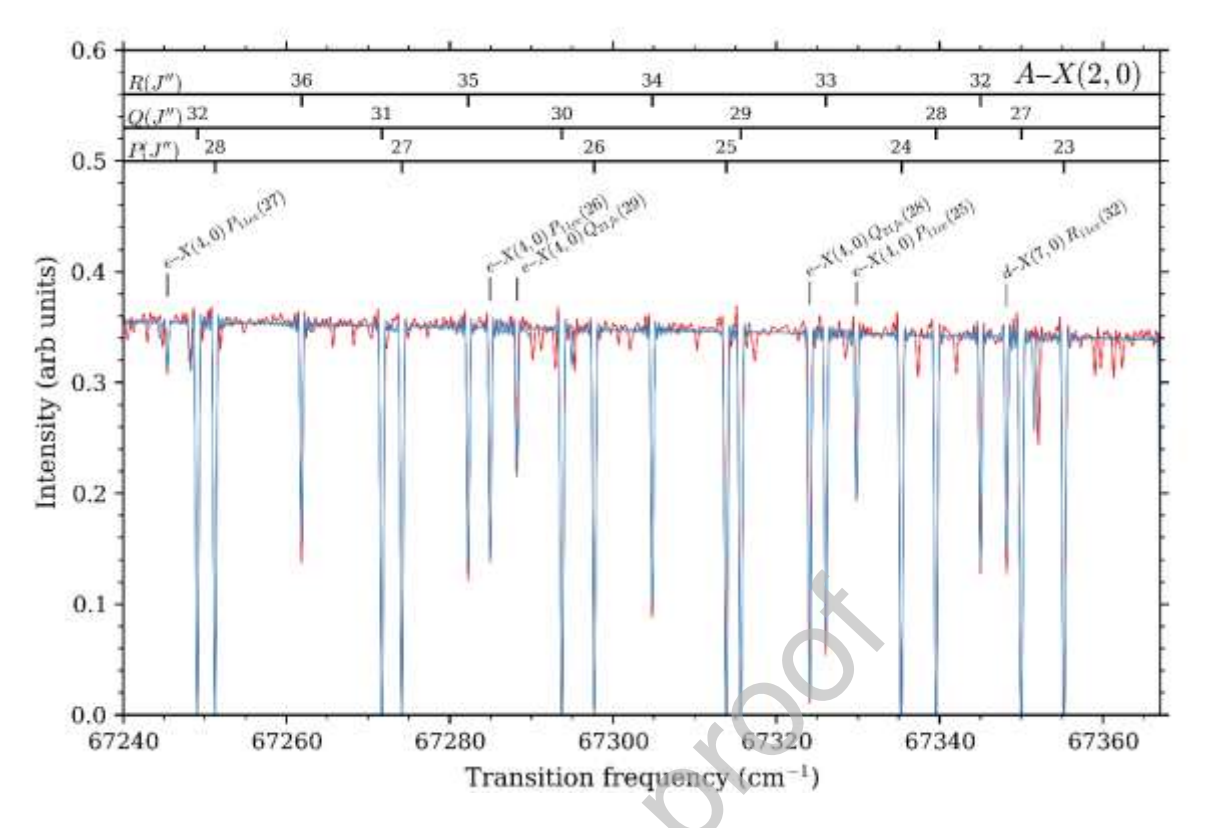


Fig. 6. Red trace: Part of the A – X(2, 0) spectrum recorded at 850 K and with a column density of 8×10^{15} cm⁻². Blue trace: Simulation of the spectrum from perturbed transition frequencies and line strengths. Main-band and extra-line assignment are given and unassigned lines are due to overlapping contamination from other CO isotopologues or absorption from X(v=1).

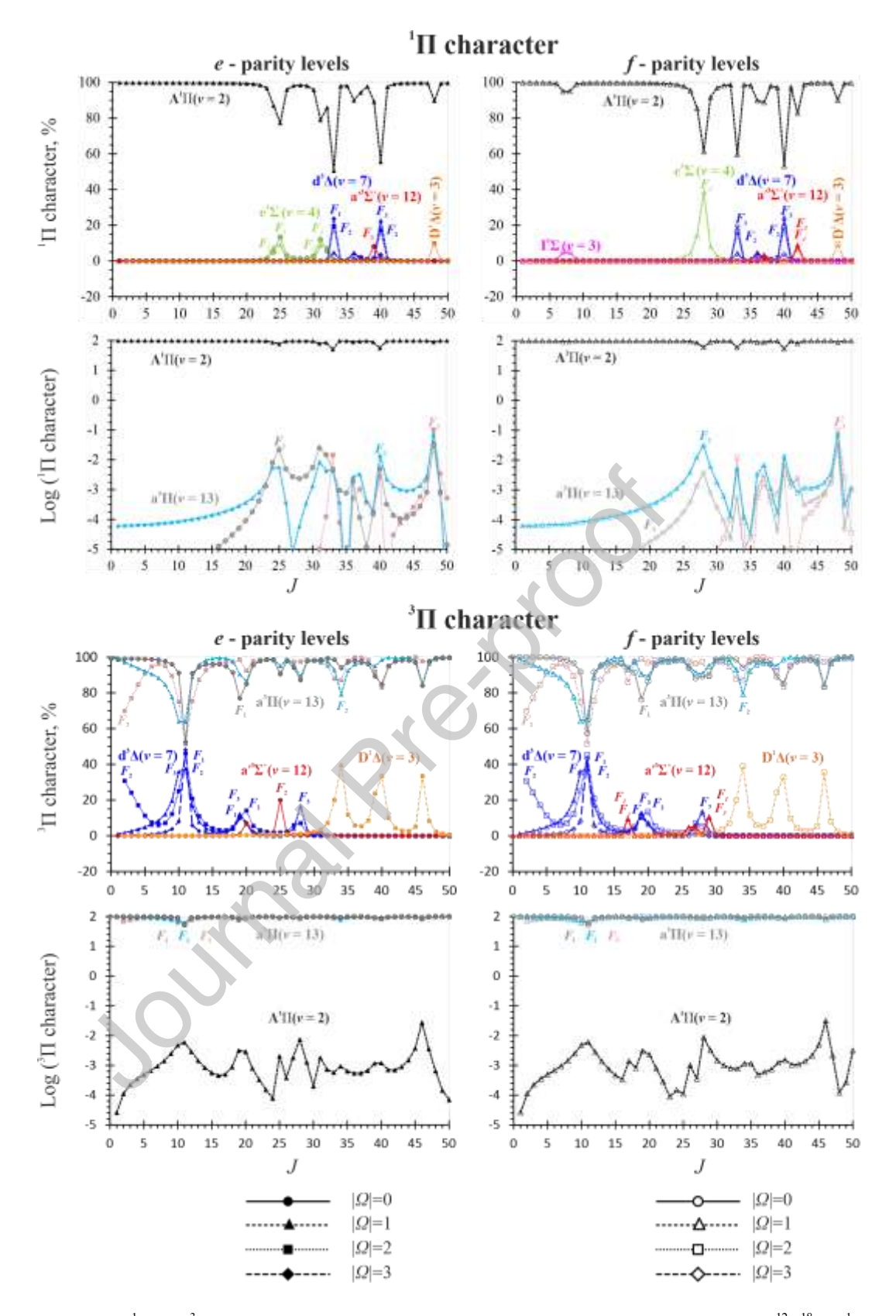


Fig. 7. Percentage ${}^{1}\Pi$ and ${}^{3}\Pi$ character of levels significantly contributing to the indirect interaction of ${}^{12}C^{18}O$ $A^{1}\Pi(\nu=2)$ and $a^{3}\Pi(\nu=13)$. The lower graphs for each case show the indirect $A^{1}\Pi \sim a^{3}\Pi$ mixing following from the $e^{3}\Sigma^{-}(\nu=4)$, $d^{3}\Delta(\nu=7)$, $a^{3}\Sigma^{+}(\nu=12)$, $D^{1}\Delta(\nu=3)$ and $I^{1}\Sigma^{-}(\nu=3)$ intermediate states (see Table 6 for details). Note that the spin states are differentiated by colour for $a^{3}\Pi(\nu=13)$, which is not the case for the rest of the electronic states.

CRediT authorship contribution statement

M. I. Malicka: Methodology, Investigation, Formal analysis, Data curation, Validation, Software, Writing - original draft, Writing - review & editing, Visualization. S. Ryzner: Visualization, Software, Formal analysis, Data curation. A. N. Heays: Conceptualization, Methodology, Investigation, Writing - original draft, Writing - review & editing, Methodology, Software, Validation, Data curation, Formal analysis, Visualization, Funding acquisition. N. de Oliveira: Investigation, Software, Validation, Writing - original draft, Writing - review & editing. R. W. Field: Conceptualization, Methodology (specialist on perturbations in general and, specifically, in CO), Validation, Resources, Writing - review & editing, Funding acquisition. W. Ubachs: Conceptualization, Investigation, Methodology, Validation, Writing - review & editing, Resources, Funding acquisition. R. Hakalla: Conceptualization, Supervision, Funding acquisition, Project administration, Methodology, Software, Investigation, Formal analysis, Validation, Resources, Writing - original draft, Writing - review & editing.

Declaration of interests

☑ The authors declare that they have no known competing financial interests or personal relationships that could have appeared to influence the work reported in this paper.